Spin-gap formation in bilayer cuprates due to enhanced interlayer pairing

Menke U. Ubbens and Patrick A. Lee
Department of Physics, Massachusetts Institute of Technology, Cambridge, Massachusetts 02139
(Received 16 December 1993)

We study a model for a pair of copper-oxide planes, described by the t-J model with a small interplane exchange term $J_\perp \mathbf{S}_i^{(1)} \cdot \mathbf{S}_i^{(2)}$. We show that this interplane interaction can be responsible for some of the unusual properties of multilayer high-T_c cuprates. An important role is played by antiferromagnetic spin correlations, causing strong peaks in the susceptibility $\chi^{\mathrm{RPA}}(\mathbf{q}, q_z)$ at the incommensurate nesting vectors $\mathbf{Q}_{\mathrm{AF}} \simeq (\pi, \pi \pm 2x)$. Consequently the effective coupling constants $J_\parallel^{\mathrm{eff}}(\mathbf{q})$ and $J_\perp^{\mathrm{eff}}(\mathbf{q})$ are also peaked at $\mathbf{q} = \mathbf{Q}_{\mathrm{AF}}$. We show that this leads to strongly enhanced interplane pairing between fermions on adjacent CuO_2 planes, characterized by a pairing order parameter $\Delta_\perp(\mathbf{r}_{ij}) = \langle f_{i\uparrow}^{(1)} f_{j\downarrow}^{(2)} - f_{i\downarrow}^{(1)} f_{j\uparrow}^{(2)} \rangle$ which extends over several lattice spacings. We find that $\Delta_\perp(\mathbf{k})$ has an (extended) s-wave symmetry and is peaked at the corners of the Fermi surface. We give qualitative arguments why the gauge field, which at low doping is very effective in destroying the in-plane pairing $\Delta_\parallel$, is less effective in destroying the interplane pairing. This leads to the conclusion that $\Delta_\perp(\mathbf{k})$ can be responsible for the observed spin-gap phase in bilayer cuprates. We use this model to calculate the NMR-relaxation rate, the echo-decay rate, and the Knight shift. Our numerical results are in qualitative agreement with the experimental data on $YBa_2Cu_3O_{6.6}$. We also suggest that the superconducting state in bilayer materials is a combination of d-wave pairing in the plane and s-wave pairing between planes. In heavily underdoped materials where the spin gap is large, the interplane pairing may dominate and a nodeless gap structure is predicted.

I. INTRODUCTION

Since the early days of high-T_c superconductivity physicists have focused on the copper-oxide planes to explain the unusual properties of the high-T_c cuprates. A widely accepted point of view is that the structure between the CuO_2 planes can be considered as a charge reservoir, whose only role is to fix a certain charge density in the CuO_2 planes. Consequently many theoretical models for the cuprates, such as the t-J model and the Hubbard model, are actually models for a *single* CuO_2 plane, ignoring the exchange coupling between the layers. This is appropriate for single-layer materials such as $La_{2-x}Sr_xCuO_4$, where the interlayer coupling is frustrated because the CuO_2 layers are shifted relative to each other. However, this is not the case for bilayer materials such as $YBa_2Cu_3O_{7-\delta}$, because the two CuO_2 planes in each bilayer are directly on top of each other, giving rise to an unfrustrated exchange coupling between the two planes.

Experiments indicate that there is a significant difference between the physical properties of single-layer materials and the properties of multilayer materials. For instance, it is well known that the superconducting transition temperature is in general higher for compounds that have more CuO_2 planes in a unit cell. Another difference is that in multilayer materials such as $YBa_2Cu_3O_{6.6}$ one observes a *spin gap* in experiments that probe the spin degrees of freedom of the electrons.[1–3] This spin-gap phase is observed at low doping and survives well above the superconducting transition temperature. According to a recent analysis of the experimental data,[4] the spin-gap phase is only observed in multilayer materials but not in single-layer materials. It is then plausible that the spin gap is directly related to the pairing of electrons on nearby CuO_2 planes.[4,5]

Before considering a model for coupled CuO_2 planes, we will first briefly discuss the physics of a single CuO_2 plane. A single CuO_2 plane can be described by the t-J model,[6] which has been studied extensively in previous articles using the slave-boson gauge-field approach.[7–13] In this approach the physical electrons are split into fermions and bosons (sometimes called *spinons* and *holons*) that interact which each other via a fluctuating gauge field. The superconducting phase is the phase in which the fermions have formed Cooper pairs, while the bosons are Bose condensed at the same time. It was suggested that the spin-gap phase corresponds to the situation in which the fermions have formed Cooper pairs, but the bosons are not Bose condensed yet.[8–10,14,15] In a recent article we showed that this picture is modified significantly by the fluctuating gauge field, which is very effective in destroying the formation of Cooper pairs at low doping.[12] As a result the superconducting transition temperature is suppressed at low doping and the spin-gap phase disappears completely. After including the pair-breaking effects of the gauge field the superconducting phase diagram that we obtained corresponds very well with the actual phase diagram of the single-layer high-T_c cuprates. We conclude that the two-dimensional t-J model is succesful in explaining the phase diagram of single-layer cuprates, but is not able to explain certain features of multilayer materials, such as the spin-gap phase.

In this paper we consider a model for two coupled CuO_2 planes, where each plane is described by the two-

dimensional t-J model. In addition we include a small antiferromagnetic spin interaction between the two planes of the form $J_\perp^0 \sum_i \mathbf{S}_i^{(1)} \cdot \mathbf{S}_i^{(2)}$. This model is similar to a model studied by Millis and Monien.[4] The antiferromagnetic interlayer coupling is responsible for the fact that close to half filling the spins on nearby CuO_2 planes are locked in an antiparallel orientation. Experimentalists have not been able to determine the exact value of $J_\perp^0$, but Tranquada *et al.*[1] and Shamoto *et al.*[3] have reported a lower limit of 8 meV for $J_\perp^0$. Because the interplane coupling is much smaller than the in-plane coupling, one would naively expect that the interplane coupling is completely irrelevant for the pairing mechanism of the high-T_c cuprates. We will argue however, that due to strong antiferromagnetic spin correlations the *effective* interplane coupling $J_\perp^{\rm eff}(\mathbf{r})$ is strongly enhanced, and extends over a coherence length of several lattice spacings. The picture that we have in mind is that the spins in each plane are correlated in patches that consist of several spins, so that effectively there is a coupling of correlated patches of spins on adjacent planes. This is clearly a much stronger coupling than the original coupling of single spins. The method that we use to take the antiferromagnetic (AF) correlation of the spins into account is the random-phase approximation (RPA).

Our main conclusion is that the enhanced interplane coupling $J_\perp^{\rm eff}(\mathbf{r})$ leads to strongly enhanced pairing between fermions on different planes, described by the interplane order parameter $\Delta_\perp(\mathbf{r}_{ij}) = \langle f_{i\uparrow}^{(1)} f_{j\downarrow}^{(2)} - f_{i\downarrow}^{(1)} f_{j\uparrow}^{(2)} \rangle$. The possibility of interplane pairing has been discussed earlier by Altshuler and Ioffe.[5] We find that due to the antiferromagnetic spin correlations the order parameter $\Delta_\perp(\mathbf{r}_{ij})$ extends over a coherence length of several lattice spacings. Our calculations show that the interplane gap $\Delta_\perp(\mathbf{k})$ has an extended s-wave symmetry (without nodes), and is peaked at the corners of the Fermi surface. This should be contrasted to the in-plane gap $\Delta_\parallel(\mathbf{k})$, which has a d-wave symmetry with nodes at four points on the Fermi surface.

We propose that the interplane gap $\Delta_\perp(\mathbf{k})$ is responsible for the observed spin-gap phase in multilayer cuprates, which had been suggested earlier by Millis and Monien.[4] An objection against their work has been that $J_\perp^0$ is much too small to explain the spin gap in $YBa_2Cu_3O_{6.6}$. We avoided this problem with the argument that at low doping $J_\perp^{\rm eff}$ is strongly enhanced by antiferromagnetic correlations. This leaves the question why we cannot apply the same argument to create a spin gap using the *in-plane* coupling $J_\parallel^{\rm eff}$, which is still larger than the interplane coupling $J_\perp^{\rm eff}$. This is partly explained by the fact that $J_\perp^{\rm eff}$ is much more enhanced than $J_\parallel^{\rm eff}$. However, for a complete answer we have to go beyond mean-field theory, and discuss the pair-breaking effects of the gauge field in the t-J model. In a previous paper we showed that at low doping the in-plane gap $\Delta_\parallel(\mathbf{k})$ is destroyed by gauge field fluctuations,[12] so that the in-plane pairing cannot give rise to a spin-gap phase. We expect that the gauge field is less effective in destroying the interplane gap $\Delta_\perp(\mathbf{k})$. This difference, which will be discussed in greater detail in Sec. V, can be understood as follows. The pair-breaking effect of a gauge field is related to the question whether or not a gap Δ breaks the gauge symmetry in the system. In the case of an in-plane gap $\Delta_\parallel(\mathbf{k})$ the gauge symmetry is completely broken, while in the case of an interplane gap $\Delta_\perp(\mathbf{k})$ there is still a gauge symmetry left in the system, corresponding to a massless out-of-phase gauge-field mode. As a result the interplane gap $\Delta_\perp(\mathbf{k})$ can survive above the Bose-condensation temperature, explaining the spin-gap phase in multilayer cuprates.

II. RPA ANALYSIS OF TWO COUPLED CuO_2 PLANES

In this paper we study a system of two coupled CuO_2 planes, which is a simple model for a bilayer high-T_c cuprate such as YBCO. We describe each individual plane with the two-dimensional t-J model, and in addition we include an antiferromagnetic spin coupling between the electrons on neighboring planes. This gives the Hamiltonian[1,4,16]

$$H = H_{t\text{-}J_\parallel}^{(1)} + H_{t\text{-}J_\parallel}^{(1)} + J_\perp^0 \sum_i \mathbf{S}_i^{(1)} \cdot \mathbf{S}_i^{(2)}, \tag{1}$$

where $H_{t\text{-}J}^{(n)}$ is the usual t-J Hamiltonian on plane n (n = 1 or 2), and $\mathbf{S}_i^{(n)} = c_{i\alpha}^{(n)\dagger} \boldsymbol{\sigma}_{\alpha\beta} c_{i\beta}^{(n)}$ is the spin operator of the electron $c_{i\alpha}^{(n)\dagger}$ at site i on plane n. Notice that we did not include any interlayer hopping in the Hamiltonian in Eq. (1). We will return to address this issue in Sec. VII. Typical values for the parameters t, $J_\parallel^0$ and $J_\perp^0$ are

$$\begin{aligned} t &\simeq 0.4 \text{ eV}, \\ J_\parallel^0 &\simeq 0.12 \text{ eV}, \\ J_\perp^0 &\gtrsim 0.01 \text{ eV}. \end{aligned} \tag{2}$$

The exact value of the interlayer exchange $J_\parallel^0$ is still unknown, but a lower limit of 8 meV has been reported by Tranquada *et al.*[1] and Shamoto *et al.*[3] This lower limit was obtained by studying the (absence of) optical spin-wave modes in undoped cuprates in neutron scattering experiments.

At low doping the motion of the electrons on each plane is controlled by the few empty sites. In order to take this physics into account we will employ the slave-boson approach, in which the original electron operator $c_{i\sigma}^\dagger$ is replaced by $f_{i\sigma}^\dagger b_i$, where $f_{i\sigma}^\dagger$ is a fermion operator carrying the spin of the electron, and b_i is a boson operator that keeps track of the empty sites, carrying the charge of the electron.[17–20] In the slave-boson approach the t-$J_\parallel$ Hamiltonian takes the form

$$\begin{aligned} H_{t\text{-}J_\parallel} = &-t \sum_{\langle i,j \rangle} \left(f_{i\sigma}^\dagger b_i b_j^\dagger f_{j\sigma} + \text{c.c.} \right) \\ &+ J_\parallel^0 \sum_{\langle i,j \rangle} \left(\mathbf{S}_i \cdot \mathbf{S}_j - \tfrac{1}{4} n_i n_j \right), \end{aligned} \tag{3}$$

where $\mathbf{S}_i = f_{i\alpha}^\dagger \boldsymbol{\sigma}_{\alpha\beta} f_{i\beta}$ is the spin of the electron on site i.

We will use a Hubbard-Stratonovich transformation to decouple the various terms in this Hamiltonian. The interaction term $\mathbf{S}_i \cdot \mathbf{S}_j$ can be decoupled in various different channels. The most common decoupling is in the particle-hole channel by writing

$$\mathbf{S}_i \cdot \mathbf{S}_j = -\tfrac{1}{2}(f^\dagger_{i\sigma} f_{j\sigma})(f^\dagger_{j\sigma} f_{i\sigma}) - \tfrac{1}{4} n_i n_j + \tfrac{1}{2} n_i. \tag{4}$$

This decoupling gives rise to terms of the form $\xi_{ij} f^\dagger_{i\sigma} f_{j\sigma}$ in the Hamiltonian, where ξ_{ij} is a tight-binding-like resonating-valence-bond (RVB) order parameter.[6] The disadvantage of this decoupling is that it does not take the antiferromagnetic correlations of the spins into account explicitly. In order to take the antiferromagnetic correlations into account it is more appropriate to keep terms of the form $\mathbf{S}_i \cdot \mathbf{S}_j$ in the Hamiltonian, which can be treated perturbatively to include the effect of the spin correlations.[21] In order to avoid double counting we write the Hamiltonian in Eq. (3) as

$$H_{t\text{-}J_\parallel} = H_{t\text{-}\frac{1}{2}J_\parallel} + \tfrac{1}{2} J^0_\parallel \sum_{\langle i,j \rangle} \left(\mathbf{S}_i \cdot \mathbf{S}_j - \tfrac{1}{4} n_i n_j \right), \tag{5}$$

and treat the first term using an RVB mean field ξ_{ij} and the second term using RPA. This admittedly *ad hoc* decomposition will affect the numerical factors in our results, but not the qualitative conclusions. We decouple $H_{t\text{-}\frac{1}{2}J_\parallel}$ in the particle-hole channel to obtain

$$H_{t\text{-}\frac{1}{2}J_\parallel} = \tfrac{1}{4} J^0_\parallel \sum_{\langle i,j \rangle} \left[|\xi_{ij}|^2 - \xi_{ij} \left(f^\dagger_{i\sigma} f_{j\sigma} + \frac{4t}{J_\parallel} b^\dagger_i b_j \right) - \text{c.c.} \right] + \frac{4t^2}{J_\parallel} \sum_{\langle i,j \rangle} b^\dagger_i b_j b^\dagger_j b_i. \tag{6}$$

At this point the analysis is still exact if one integrates over all configurations of the RVB field $\xi_{ij}(\tau)$. In the mean-field approximation the field ξ_{ij} is replaced by its saddle point

$$\xi = \left\langle f^\dagger_{i\sigma} f_{j\sigma} + \frac{4t}{J_\parallel} b^\dagger_i b_j \right\rangle. \tag{7}$$

The total Hamiltonian for the fermionic degrees of freedom then takes the form

$$H = \sum_{\mathbf{k}} \epsilon_{\mathbf{k}} \left(f^{(1)\dagger}_{\mathbf{k}\sigma} f^{(1)}_{\mathbf{k}\sigma} + f^{(2)\dagger}_{\mathbf{k}\sigma} f^{(2)}_{\mathbf{k}\sigma} \right) + H_{\mathrm{I}}, \tag{8}$$

where $\epsilon_{\mathbf{k}} = -\frac{1}{2} J^0_\parallel \xi (\cos k_x + \cos k_y) - \mu_F$. The interaction Hamiltonian H_{I} is given by

$$H_{\mathrm{I}} = \tfrac{1}{2} \sum_{(i,j),n,n'} J^0_{nn'}(\mathbf{r}_{ij}) \mathbf{S}^{(n)}_i \cdot \mathbf{S}^{(n')}_j = \tfrac{1}{2} \sum_{\mathbf{q},n,n'} J^0_{nn'}(\mathbf{q}) \mathbf{S}^{(n)}_{\mathbf{q}} \cdot \mathbf{S}^{(n')}_{-\mathbf{q}}, \tag{9}$$

where $J^0_{nn}(\mathbf{q}) = \tilde{J}^0_\parallel(\mathbf{q}) = J^0_\parallel(\cos q_x + \cos q_y)$ and $J^0_{nn'}(\mathbf{q}) = \tilde{J}^0_\perp(q_z) = J^0_\perp e^{iq_z d}$, and d denotes the distance between the two planes. It is convenient to write H_{I} explicitly in terms of the fermion operators $f^{(n)}_{\mathbf{k}\sigma}$:

$$H_{\mathrm{I}} = \tfrac{1}{4} \sum_{\mathbf{q},n,n'} J^0_{nn'}(\mathbf{q}) \begin{pmatrix} \uparrow\uparrow \\ \downarrow\downarrow \\ \uparrow\downarrow \\ \downarrow\uparrow \end{pmatrix}^\dagger_{\mathbf{q},n} \begin{bmatrix} \frac{1}{2} & \frac{1}{2} & 0 & 0 \\ \frac{1}{2} & \frac{1}{2} & 0 & 0 \\ 0 & 0 & 1 & 0 \\ 0 & 0 & 0 & 1 \end{bmatrix} \times \begin{pmatrix} \uparrow\uparrow \\ \downarrow\downarrow \\ \uparrow\downarrow \\ \downarrow\uparrow \end{pmatrix}_{-\mathbf{q},n'}, \tag{10}$$

where $(\uparrow\uparrow)_{\mathbf{q},n}$ denotes $\sum_{\mathbf{k}} f^{(n)\dagger}_{\mathbf{k}+\mathbf{q}/2,\uparrow} f^{(n)}_{\mathbf{k}-\mathbf{q}/2,\uparrow}$.

We will use a random-phase approximation to analyze the antiferromagnetic correlations induced by the terms in H_{I}. We will first calculate the dynamic spin susceptibility $\chi(q)$ [where q denotes $(\mathbf{q}, q_z, i\omega_n)$], which contains all the information about spin correlations. Within RPA, $\boldsymbol{\chi}^{\mathrm{RPA}}(q)$ is given by a sum over the strings of bubbles shown in Fig. 1. The susceptibility is actually an 8×8 matrix, because at each vertex of a bubble the fermion can be either on plane 1 or on plane 2, and in addition there are four possible spin combinations at each vertex ($\uparrow\uparrow$, $\downarrow\downarrow$, $\uparrow\downarrow$ or $\downarrow\uparrow$). We can safely suppress the spin indices, because every power of the 4×4 spin matrix in Eq. (10) yields the same matrix again. This leaves us with simple 2×2 matrices, where the index denotes whether the fermion is on plane 1 or 2. The susceptibility is then given by the matrix sum

$$\boldsymbol{\chi}^{\mathrm{RPA}}(q) = \chi^0(q) \sum_{m=0}^{\infty} \left[-\tfrac{1}{4} \mathbf{J}^0(q) \chi^0(q) \right]^m, \tag{11}$$

where $\chi^0(q)$ is the contribution of a single bubble. The matrix $\mathbf{J}^0(q)$ is given by

$$\mathbf{J}^0(q) = \begin{bmatrix} \tilde{J}^0_\parallel(q) & \tilde{J}^0_\perp(q) \\ \tilde{J}^0_\perp(q)^* & \tilde{J}^0_\parallel(q) \end{bmatrix}. \tag{12}$$

Evaluating the matrix sum in Eq. (11) gives

$$\begin{aligned} \boldsymbol{\chi}^{\mathrm{RPA}} &= \chi^0 \begin{bmatrix} 1 + \frac{1}{4}\chi^0 \tilde{J}^0_\parallel & \frac{1}{4}\chi^0 \tilde{J}^0_\perp \\ \frac{1}{4}\chi^0 \tilde{J}^{0\,*}_\perp & 1 + \frac{1}{4}\chi^0 \tilde{J}^0_\parallel \end{bmatrix}^{-1} \\ &= \frac{\chi^0}{(1 + \frac{1}{4}\chi^0 \tilde{J}^0_\parallel)^2 - |\frac{1}{4}\chi^0 \tilde{J}^0_\perp|^2} \times \begin{bmatrix} 1 + \frac{1}{4}\chi^0 \tilde{J}^0_\parallel & -\frac{1}{4}\chi^0 \tilde{J}^0_\perp \\ -\frac{1}{4}\chi^0 \tilde{J}^{0\,*}_\perp & 1 + \frac{1}{4}\chi^0 \tilde{J}^0_\parallel \end{bmatrix}. \end{aligned} \tag{13}$$

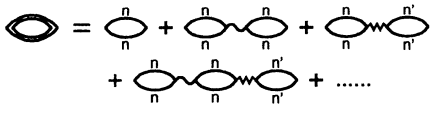

FIG. 1. The renormalized susceptibility $\chi^{\mathrm{RPA}}(q)$ in the RPA approximation. In each individual bubble the fermion can be either on plane $n = 1$ or on plane $n' = 2$. The wavy line denotes the in-plane exchange $\mathbf{S}^{(n)}_i \cdot \mathbf{S}^{(n)}_j$, and the jagged line denotes the interplane exchange $\mathbf{S}^{(n)}_i \cdot \mathbf{S}^{(n')}_i$. We show that due to antiferromagnetic correlations $\chi^{\mathrm{RPA}}(q)$ has strong incommensurate peaks at $\mathbf{q} = \mathbf{Q}_{\mathrm{AF}}$.

This expression is only valid if the eigenvalues of the matrix $\frac{1}{4}\chi^0(q)\mathbf{J}^0(q)$ are smaller than 1. Putting $i\omega_n = 0$ this leads to the inequality

$$\chi^0(\mathbf{q}) < \frac{4}{J_\perp^0 - J_\parallel^0(\cos q_x + \cos q_y)} . \tag{14}$$

At intermediate doping this inequality is usually satisfied. However, at low doping $\chi^0(\mathbf{q})$ is enhanced at the nesting vector $\mathbf{Q}_{\rm AF} \simeq (\pi,\pi)$, so that at sufficiently low doping the inequality breaks down for $\mathbf{q} \simeq \mathbf{Q}_{\rm AF}$. This indicates that at low doping the system becomes unstable against a long-range Néel order with $\langle \mathbf{S} \rangle \neq 0$.

We analyzed $\chi^{\rm RPA}(\mathbf{q})$ numerically using the parameters $t/J_\parallel^0 = 3$ and $J_\perp^0/J_\parallel^0 = 0.2$. We found that for these parameters the AF instability occurs at a doping $x \simeq 0.08$. We are mostly interested in the regime close to the AF instability, i.e., $x \gtrsim 0.08$, which is characterized by strong (incommensurate) peaks in the renormalized susceptibility $\chi^{\rm RPA}(q)$ at the nesting vector $\mathbf{q} = \mathbf{Q}_{\rm AF} \simeq (\pi, \pi \pm 2x)$. This feature of $\chi^{\rm RPA}(\mathbf{q})$ has been studied extensively by Tanamoto and co-workers for a generalized t-J model that included next-nearest-neighbor hopping terms to simulate the band structure of different cuprates.[21] Their analysis was for a single CuO_2 plane, and did therefore not include any interplane interactions. They emphasized that the critical doping x_c at which the AF instability occurs depends strongly on the details of the band structure.

The physical susceptibility that one measures in neutron scattering experiments is proportional to $\sum_{n,n'}\langle n'|\chi|n\rangle$, which gives

$$\chi^{\rm RPA}_{\rm phys}(\mathbf{q}, q_z, i\omega_n) = \left[\frac{\cos^2(\frac{1}{2}q_z d)}{1 + \frac{1}{4}\chi^0[\tilde{J}_\parallel^0(\mathbf{q}) + J_\perp^0]} + \frac{\sin^2(\frac{1}{2}q_z d)}{1 + \frac{1}{4}\chi^0[\tilde{J}_\parallel^0(\mathbf{q}) - J_\perp^0]}\right]\chi^0(\mathbf{q}, i\omega_n). \tag{15}$$

Here we used that $\tilde{J}_\perp^0(q_z) = J_\perp^0 e^{iq_z d}$. This expression shows that $\chi^{\rm RPA}_{\rm phys}(\mathbf{q}, q_z)$ has a modulation as a function of q_z with a period $2\pi/d$. The maxima occur at $q_z = \pi/d \pmod{2\pi/d}$ and the minima at $q_z = 0 \pmod{2\pi/d}$. This modulation is especially pronounced close to the AF instability with $\mathbf{q} \simeq \mathbf{Q}_{\rm AF}$. In that case the maxima can be significantly larger than the minima. This corresponds well with the neutron scattering experiments of Tranquada *et al.*, who measured $\chi''(\mathbf{Q}_{\rm AF}, q_z)$ as a function of q_z.[1] They indeed observed a modulation of period $2\pi/d$, with maxima at $q_z = \pm\pi/d$ that were approximately twice the value of the minimum at $q_z = 0$.

We will now use the expression for $\chi^{\rm RPA}(q)$ in Eq. (13) to calculate the effective spin-spin interaction, which we denote by $J_\parallel^{\rm eff}(\mathbf{q})$ and $J_\perp^{\rm eff}(\mathbf{q}, q_z)$. Within RPA the effective interaction can be written in matrix notation as

$$\mathbf{J}^{\rm eff} = \mathbf{J}^0 - \tfrac{1}{4}\mathbf{J}^0\boldsymbol{\chi}^{\rm RPA}\mathbf{J}^0, \tag{16}$$

where the 2×2 matrices $\mathbf{J}^0$ and $\boldsymbol{\chi}^{\rm RPA}$ are given by Eqs. (12) and (13). Evaluating the matrix products gives

$$J_\parallel^{\rm eff}(\mathbf{q}) = \frac{\tilde{J}_\parallel^0(\mathbf{q})\left[1 + \frac{1}{4}\chi^0\tilde{J}_\parallel^0(\mathbf{q})\right] - \frac{1}{4}\chi^0 {J_\perp^0}^2}{[1 + \frac{1}{4}\chi^0\tilde{J}_\parallel^0(\mathbf{q})]^2 - (\frac{1}{4}\chi^0 J_\perp^0)^2}, \tag{17}$$

$$\tilde{J}_\perp^{\rm eff}(\mathbf{q}, q_z) = \frac{J_\perp^0}{[1 + \frac{1}{4}\chi^0\tilde{J}_\parallel^0(\mathbf{q})]^2 - (\frac{1}{4}\chi^0 J_\perp^0)^2} e^{iq_z d}. \tag{18}$$

Note that $\tilde{J}_\perp^{\rm eff}$ always has the form $\tilde{J}_\perp^{\rm eff}(\mathbf{q}, q_z) = J_\perp^{\rm eff}(\mathbf{q})e^{iq_z d}$. Close to the AF instability $J_\parallel^{\rm eff}(\mathbf{q})$ and $J_\perp^{\rm eff}(\mathbf{q})$ are both strongly peaked at the nesting vector $\mathbf{q} = \mathbf{Q}_{\rm AF}$, and the width of this peak is related to the correlation length r_0 over which the spins are Néel ordered. Let us first study Eqs. (17) and (18) in the important limit $J_\perp^0 \ll J_\parallel^0$. In that case $J_\parallel^{\rm eff}$ is enhanced by a factor $(1+\frac{1}{4}\chi^0\tilde{J}_\parallel^0)^{-1}$, while $J_\perp^{\rm eff}$ is enhanced by the *square* of this factor. We conclude that for $\mathbf{q} \simeq \mathbf{Q}_{\rm AF}$, $J_\perp^{\rm eff}(\mathbf{q})$ is much stronger enhanced by antiferromagnetic correlations than $J_\parallel^{\rm eff}(\mathbf{q})$. It is interesting to note, however, that $J_\perp^{\rm eff}(\mathbf{q})$ will never exceed $|J_\parallel^{\rm eff}(\mathbf{q})|$, assuming that $J_\perp^0 < |\tilde{J}_\parallel^0(\mathbf{q})|$. In the limit $\frac{1}{4}\chi^0(\mathbf{q})(\tilde{J}_\parallel^0(\mathbf{q}) - J_\perp^0) \to -1$, $J_\perp^{\rm eff}$ approaches $J_\parallel^{\rm eff}(\mathbf{q})$, even if $J_\perp^0$ was initially much smaller than $\tilde{J}_\parallel^0$. This implies that close to the AF instability $J_\perp^{\rm eff}$ and $J_\parallel^{\rm eff}$ are approximately equal in strength.

We analyzed $J_\parallel^{\rm eff}(\mathbf{q})$ and $J_\perp^{\rm eff}(\mathbf{q})$ numerically using the parameters $t/J_\parallel^0 = 3$ and $J_\perp^0/J_\parallel^0 = 0.2$. We focused in particular on doping slightly above the critical doping $x_c \simeq 0.08$ at which the AF instability occurs. In Fig. 2 we show plots of $J_\parallel^{\rm eff}(\mathbf{q})$ and $J_\perp^{\rm eff}(\mathbf{q})$ for $x = 0.09$, $x = 0.12$, and $x = 0.20$. The three curves show that close to the AF instability there are strongly pronounced incommensurate peaks at $\mathbf{Q}_{\rm AF} \simeq (\pi, \pi \pm 2x)$. By analyzing this peak we find that for $x = 0.09$ the correlation length r_0 is roughly three lattice spacings, i.e., $r_0/a \simeq 3$. These

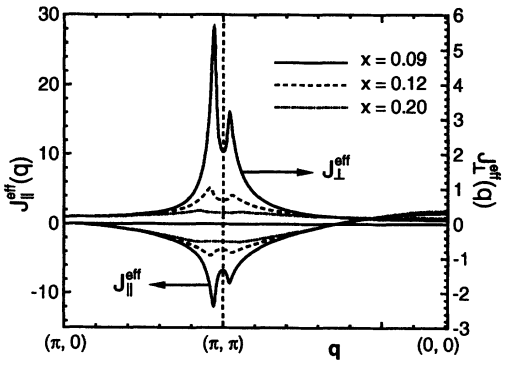

FIG. 2. The effective in-plane coupling $J_\parallel^{\rm eff}(\mathbf{q})$ (left axis) and the effective interplane coupling $J_\perp^{\rm eff}(\mathbf{q})$ (right axis) for various values of the doping x. The right axis is blown up by a factor of 5 in order to show the features of $J_\perp^{\rm eff}(\mathbf{q})$ more clearly. Close to the AF instability at $x_c = 0.08$, $J_\parallel^{\rm eff}(\mathbf{q})$ and $J_\perp^{\rm eff}(\mathbf{q})$ have strong incommensurate peaks at $\mathbf{Q}_{\rm AF} \simeq (\pi, \pi \pm 0.19)$. These peaks fade away at higher dopings $x \gg x_c$. Notice that for $x \to x_c$ the interplane coupling $J_\perp^{\rm eff}(\mathbf{Q}_{\rm AF})$ is more enhanced than $J_\parallel^{\rm eff}(\mathbf{Q}_{\rm AF})$. As a result $J_\perp^{\rm eff}$ and $J_\parallel^{\rm eff}$ become comparable in strength, even though initially $J_\perp^0 \ll J_\parallel^0$.

peaks fade away when the doping is much higher than x_c. Notice that for $x = 0.09$, $J_\perp^{\rm eff}(\mathbf{q})$ is much smaller than $J_\parallel^{\rm eff}(\mathbf{q})$ over most of the Brioullin zone, but close to the incommensurate peaks $J_\perp^{\rm eff}(\mathbf{q})$ is more strongly enhanced than $J_\parallel^{\rm eff}(\mathbf{q})$, so that the $J_\perp^{\rm eff}(\mathbf{q})$ and $J_\parallel^{\rm eff}(\mathbf{q})$ become comparable in strength at $\mathbf{q} \simeq \mathbf{Q}_{\rm AF}$. This means that the interplane coupling cannot be ignored when the spins of the electrons exhibit strong antiferromagnetic correlations.

III. INTERPLANE PAIRING

In the previous section we showed that the interplane coupling $J_\perp^{\rm eff}(\mathbf{q})$ is strongly enhanced around $\mathbf{q} \simeq \mathbf{Q}_{\rm AF}$ due to antiferromagnetic correlations. We will now show that this enhanced coupling leads to interplane pairing at a much higher energy scale than before. The physical picture that we have in mind is that the spins on both planes form patches of correlated spins, so that the system can create extended Cooper pairs that consist of patches of spins on one plane that pair up with corresponding patches of spins on the other plane. This interplane pairing is characterized by the order parameter $\Delta_\perp(\mathbf{r}_{ij}) = \langle f_{i\uparrow}^{(1)} f_{j\downarrow}^{(2)} - f_{i\downarrow}^{(1)} f_{j\uparrow}^{(2)} \rangle$.

Consider the Hamiltonian in Eq. (8), but with the bare in-plane and interplane couplings $J_\parallel^0$ and $J_\perp^0$ replaced by the effective couplings $J_\parallel^{\rm eff}$ and $J_\perp^{\rm eff}$. Each of these interaction terms can be written in the form

$$J_{nn'}^{\rm eff}(\mathbf{r}_{ij}) \left(\mathbf{S}_i^{(n)} \cdot \mathbf{S}_j^{(n')} - \tfrac{1}{4} n_i n_j \right) = -\tfrac{1}{2} J_{nn'}^{\rm eff}(\mathbf{r}_{ij}) \left(f_{i\uparrow}^{(n)\dagger} f_{j\downarrow}^{(n')\dagger} - f_{i\downarrow}^{(n)\dagger} f_{j\uparrow}^{(n')\dagger} \right) \times \left(f_{j\downarrow}^{(n')} f_{i\uparrow}^{(n)} - f_{j\uparrow}^{(n')} f_{i\downarrow}^{(n)} \right). \tag{19}$$

The coupling constants $J_{nn'}^{\rm eff}(\mathbf{r}_{ij})$ are the Fourier transforms of the functions $J_\parallel^{\rm eff}(\mathbf{q})$ and $J_\perp^{\rm eff}(\mathbf{q})$ in Eqs. (17) and (18). The terms in Eq. (19) can be decoupled in the particle-particle channel by defining a Hubbard-Stratonovich field $\Delta_{ij}^{(nn')}$ on the bond (i,j), under the condition that $J_{nn'}(\mathbf{r}_{ij}) > 0$. This gives the Hamiltonian

$$H = \sum_{\mathbf{k},n} \epsilon_k f_{\mathbf{k}\sigma}^{(n)\dagger} f_{\mathbf{k}\sigma}^{(n)} + \tfrac{1}{2} {\sum_{(in,jn')}}' J_{nn'}^{\rm eff}(\mathbf{r}_{ij}) \times \left[\left| \Delta_{ij}^{nn'} \right|^2 - \Delta_{ij}^{nn'*} \left(f_{i\uparrow}^{(n)} f_{j\downarrow}^{(n')} - f_{i\downarrow}^{(n)} f_{j\uparrow}^{(n')} \right) - \text{c.c.} \right], \tag{20}$$

where the indices n and n' denote plane 1 or 2. The prime in $\sum'$ denotes that the sum is only over the bonds (i,j) for which $J_{nn'}(\mathbf{r}_{ij}) > 0$. This means that for $J_\parallel^{\rm eff}(\mathbf{r}_{ij})$ we only include bonds (i,j) with i and j on different sublattices, while for $J_\perp^{\rm eff}(\mathbf{r}_{ij})$ we only include bonds (i,j) with i and j on the same sublattice. At the mean-field level the fields $\Delta_{ij}^{nn'}$ are replaced by their saddle points, i.e., constant values that minimize the total free energy. Assuming that $\Delta_{ij}^{nn'} = \Delta_{nn'}(\mathbf{r}_{ij})$ is real, we can write the Hamiltonian in momentum space in the matrix form

$$H = \sum_{\mathbf{k}} \begin{pmatrix} f_{\mathbf{k}\uparrow}^{(1)} \\ f_{-\mathbf{k}\downarrow}^{(1)\dagger} \\ f_{\mathbf{k}\uparrow}^{(2)} \\ f_{-\mathbf{k}\downarrow}^{(2)\dagger} \end{pmatrix}^\dagger \begin{bmatrix} \epsilon_{\mathbf{k}} & \Delta_\parallel & 0 & \Delta_\perp \\ \Delta_\parallel & -\epsilon_{\mathbf{k}} & \Delta_\perp & 0 \\ 0 & \Delta_\perp & \epsilon_{\mathbf{k}} & \Delta_\parallel \\ \Delta_\perp & 0 & \Delta_\parallel & -\epsilon_{\mathbf{k}} \end{bmatrix} \begin{pmatrix} f_{\mathbf{k}\uparrow}^{(1)} \\ f_{-\mathbf{k}\downarrow}^{(1)\dagger} \\ f_{\mathbf{k}\uparrow}^{(2)} \\ f_{-\mathbf{k}\downarrow}^{(2)\dagger} \end{pmatrix} + {\sum_{\mathbf{r}}}' \left[J_\parallel^{\rm eff}(\mathbf{r}) \Delta_\parallel(\mathbf{r})^2 + J_\perp^{\rm eff}(\mathbf{r}) \Delta_\perp(\mathbf{r})^2 \right], \tag{21}$$

where

$$\epsilon_{\mathbf{k}} = -\tfrac{1}{2} \xi J_\parallel^0 (\cos k_x + \cos k_y) - \mu_F, \tag{22}$$

$$\Delta_\parallel(\mathbf{k}) = {\sum_{\mathbf{r}}}' \cos(\mathbf{k}\cdot\mathbf{r}) J_\parallel^{\rm eff}(\mathbf{r}) \Delta_\parallel(\mathbf{r}), \tag{23}$$

$$\Delta_\perp(\mathbf{k}) = {\sum_{\mathbf{r}}}' \cos(\mathbf{k}\cdot\mathbf{r}) J_\perp^{\rm eff}(\mathbf{r}) \Delta_\perp(\mathbf{r}). \tag{24}$$

The sum $\sum_{\mathbf{r}}'$ denotes a sum over bonds, which means that $\mathbf{r}$ and $-\mathbf{r}$ should be counted only once and $\mathbf{r} = 0$ is counted half. The Hamiltonian in Eq. (21) can easily be diagonalized, which gives the quasiparticle energy dispersion

$$E_\pm(\mathbf{k}) = \sqrt{\epsilon_{\mathbf{k}}^2 + \Delta_\pm(\mathbf{k})^2}, \tag{25}$$

$$\Delta_\pm(\mathbf{k}) = \Delta_\parallel(\mathbf{k}) \pm \Delta_\perp(\mathbf{k}). \tag{26}$$

The order parameters $\Delta_\parallel(\mathbf{r})$ and $\Delta_\perp(\mathbf{r})$ are determined by the condition that the free energy is at a local minimum. The free energy is given by

$$F = {\sum_{\mathbf{r}}}' \left[J_\parallel^{\rm eff}(\mathbf{r}) \Delta_\parallel(\mathbf{r})^2 + J_\perp^{\rm eff}(\mathbf{r}) \Delta_\perp(\mathbf{r})^2 \right] - 2T \sum_{s=\pm} \int \frac{d^2k}{(2\pi)^2} \ln\left[\cosh(E_s(\mathbf{k})/2T) \right]. \tag{27}$$

Putting $\partial F / \partial \Delta^{nn'}(\mathbf{r}) = 0$ for all $\Delta^{nn'}(\mathbf{r})$, we obtain the following set of self-consistency equations:

$$\Delta_{nn'}(\mathbf{r}) = \sum_{s=\pm 1} \int \frac{d^2k}{(2\pi)^2} \cos(\mathbf{k}\cdot\mathbf{r}) \left(\frac{s^{n-n'} \Delta_s(\mathbf{k})}{E_s(\mathbf{k})} \right) \times \tanh\left(\frac{E_s(\mathbf{k})}{2T} \right). \tag{28}$$

This set of self-consistency equations has in general several solutions, depending on the symmetry that one chooses for the order parameter, i.e., the relative signs of the order parameters $\Delta_{nn'}(\mathbf{r})$ on different bonds $\mathbf{r}$. Close to half filling one can find the most favorable symmetry of the order parameter, by studying the free energy in Eq. (27) in the limit $\Delta_{nn'}(\mathbf{r}) \to 0$. This gives

$$F(\Delta) - F(0) = {\sum_{\mathbf{r}}}' \left[J_\parallel^{\rm eff}(\mathbf{r}) \Delta_\parallel(\mathbf{r})^2 + J_\perp^{\rm eff}(\mathbf{r}) \Delta_\perp(\mathbf{r})^2 \right] - \int \frac{d^2k}{(2\pi)^2} \left[\Delta_\parallel(\mathbf{k})^2 + \Delta_\perp(\mathbf{k})^2 \right] \times \frac{\tanh(\epsilon_{\mathbf{k}}/2T)}{\epsilon_{\mathbf{k}}}. \tag{29}$$

The gain in free energy is largest if all the terms in the expression for $\Delta_{nn'}(\mathbf{k})$ in Eqs. (23) and (24) add constructively for the momenta $\mathbf{k}$ that give the largest contribution to the integral in Eq. (29). Close to half filling the momentum integral in Eq. (29) is dominated by the $\mathbf{k}$ vectors at the four corners of the Fermi surface, i.e., the points $\mathbf{k} = (\pm\pi, 0)$ and $\mathbf{k} = (0, \pm\pi)$, because close to half filling the density of states diverges at those four points. At the corner $\mathbf{k} = (\pi, 0)$ the gap $\Delta_{nn'}(\mathbf{k})$ is given by

$$\Delta_{nn'}(\pi, 0) = \sum_{\mathbf{r}}{}' (-1)^{r_x} J_{nn'}(\mathbf{r}) \Delta_{nn'}(\mathbf{r}). \tag{30}$$

Because the summation $\sum_{\mathbf{r}}'$ is only over vectors $\mathbf{r}$ for which $J_{nn'}(\mathbf{r})$ is positive, the terms in Eq. (30) add constructively if we let the sign of $\Delta_{nn'}(\mathbf{r})$ alternate depending on whether r_x and r_y are even or odd. We will measure r_x and r_y in units of the lattice constant a. To be more explicit, the gain in free energy is largest if we choose

$$\Delta_{\parallel}(\mathbf{r}) = \begin{cases} > 0 & \text{for } r_x \text{ even and } r_y \text{ odd,} \\ < 0 & \text{for } r_x \text{ odd and } r_y \text{ even,} \\ = 0 & \text{for } r_x + r_y \text{ even,} \end{cases} \tag{31}$$

$$\Delta_{\perp}(\mathbf{r}) = \begin{cases} > 0 & \text{for } r_x \text{ and } r_y \text{ even,} \\ < 0 & \text{for } r_x \text{ and } r_y \text{ odd,} \\ = 0 & \text{for } r_x + r_y \text{ odd.} \end{cases} \tag{32}$$

Notice that $\Delta_{\parallel}(r_x, r_y) = -\Delta_{\parallel}(r_y, r_x)$ and $\Delta_{\perp}(r_x, r_y) = +\Delta_{\perp}(r_y, r_x)$. This implies that $\Delta_{\perp}(\mathbf{k})$ has an extended s-wave symmetry [i.e., $\Delta_{\perp}(\mathbf{k}) = \Delta_{\perp}(\mathbf{k}_{\perp})$ for $\mathbf{k}_{\perp} = (k_y, k_x)$], while $\Delta_{\parallel}(\mathbf{k})$ has an extended d-wave symmetry [i.e., $\Delta_{\parallel}(\mathbf{k}) = -\Delta_{\parallel}(\mathbf{k}_{\perp})$]. The prefix "extended" indicates that $\Delta_{\perp}(\mathbf{k})$ and $\Delta_{\parallel}(\mathbf{k})$ can be anisotropic around the Fermi surface, with peaks at the corners $(\pm\pi, 0)$ and $(0, \pm\pi)$. This should be contrasted to a *pure* s-wave symmetry [$\Delta_{\perp}(\mathbf{k}) = \text{const}$] or a pure d-wave symmetry [$\Delta_{\parallel}(\mathbf{k}) \propto \cos k_x - \cos k_y$].

We can now explain why superconductivity is enhanced when the effective coupling $J^{\text{eff}}(\mathbf{r})$ extends over several lattice spacings. Suppose that $J^{\text{eff}}(\mathbf{r})$ falls off over a correlation length r_0, for example, $J^{\text{eff}}(\mathbf{r}) = J^0 e^{-r/r_0}$. In that case there are of the order of r_0^2 terms $\Delta(\mathbf{r})$ that add constructively in the expression for the gap $\Delta(\mathbf{k})$ in Eq. (30) for $\mathbf{k} = (\pm\pi, 0)$ or $(0, \pm\pi)$. Therefore the second term in the free energy in Eq. (29), which corresponds to a *gain* of free energy, is essentially enhanced by a factor r_0^4. On the other hand the first term in Eq. (29), which corresponds to a *cost* of free energy, is only enhanced by a factor r_0^2. We therefore obtain a net gain of free energy which becomes larger and larger if the correlation length r_0 increases. As a result superconductivity is enhanced. We would like to emphasize that our arguments for the behavior of $\Delta_{\parallel}(\mathbf{k})$ and $\Delta_{\perp}(\mathbf{k})$ are only valid close to half filling, and under the condition that $T \ll J$ and $\Delta(\mathbf{k}) \ll J$. These conditions are needed to make sure that the momentum integrals in Eqs. (28) and (29) are dominated by the corners of the Fermi surface. Away from half filling the corners of the Fermi surface become progressively less important, and therefore superconductivity will not be as strongly enhanced in that case.

From this point on we will focus on the order parameter $\Delta_{\perp}(\mathbf{r})$, and ignore $\Delta_{\parallel}(\mathbf{r})$. The motivation for this is twofold. The first reason is that the interplane order parameter $\Delta_{\perp}$ is more efficient in taking advantage of the antiferromagnetic correlations than $\Delta_{\parallel}$, which is partly due to the fact that $J_{\perp}^{\text{eff}}(\mathbf{q})$ is stronger peaked at $\mathbf{q} = \mathbf{Q}_{\text{AF}}$ than $J_{\parallel}^{\text{eff}}(\mathbf{q})$, as we explained after Eq. (18). But our main motivation for ignoring $\Delta_{\parallel}$ is that the gauge field is very effective in destroying the in-plane gap $\Delta_{\parallel}(\mathbf{k})$ at low doping.[12] This is the region we are interested in, because the spin-gap phase is observed at low doping. We anticipate that the gauge field is less effective in destroying the interplane gap $\Delta_{\perp}(\mathbf{k})$, which we will discuss in more detail in Sec. V.

IV. NUMERICAL ANALYSIS OF INTERPLANE PAIRING

The numerical results presented in this section are meant for underdoped cuprates in the spin-gap phase. Within our model this corresponds to the situation in which $\Delta_{\perp}$ is finite, but $\Delta_{\parallel} = 0$. We solved the self-consistency equations for $\Delta_{\perp}(\mathbf{r})$ in Eq. (28), using the RPA-enhanced interplane coupling $J_{\perp}^{\text{eff}}(\mathbf{r})$ that we calculated in Sec. II. We performed the calculations at a doping $x = 0.085$, which is close to the AF instability at $x \simeq 0.08$. In this calculation we assumed $J_{\perp}^0 = 0.2\, J_{\parallel}^0$. For this amount of doping $J_{\perp}^{\text{eff}}(\mathbf{r})$ falls off over a correlation length of approximately three to four lattice spacings, which is quite typical for high-T_c cuprates in the spin-gap phase.

In Fig. 3 we show a plot of $(-1)^{r_x}\Delta_{\perp}(\mathbf{r})$ versus $|\mathbf{r}|$ for the discrete set of bonds on which $\Delta_{\perp}(\mathbf{r})$ is defined; i.e., $r_x + r_y$ is even. Note that $\Delta_{\perp}(\mathbf{r})$ falls off over a coherence length of approximately three to four lattice spacings, and that $\Delta_{\perp}(\mathbf{r})$ is positive on the sublattice with r_x even

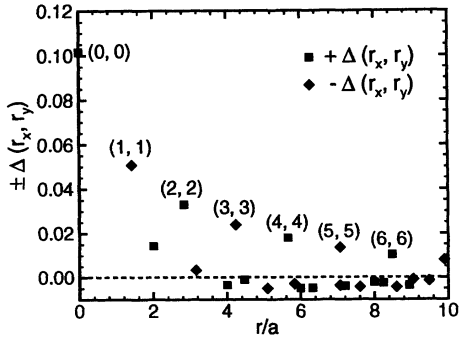

FIG. 3. The pairing order parameter $\Delta_{\perp}(\mathbf{r})$ for $x = 0.085$. Due to the antiferromagnetic correlations $\Delta_{\perp}(\mathbf{r})$ is also nonzero for $\mathbf{r} \neq 0$, and $\Delta_{\perp}(\mathbf{r})$ decays over a correlation length of approximately three to four lattice spacings. Notice that $\Delta_{\perp}(\mathbf{r})$ alternates sign from one sublattice to the next, as indicated by the squares $(+\Delta_{\perp})$ and the diamonds $(-\Delta_{\perp})$. Also notice that $\Delta_{\perp}(\mathbf{r})$ is relatively strong along the diagonals $r_x = \pm r_y$. This implies that in momentum space $\Delta_{\perp}(\mathbf{k})$ is enhanced around the diamond-shaped Fermi surface.

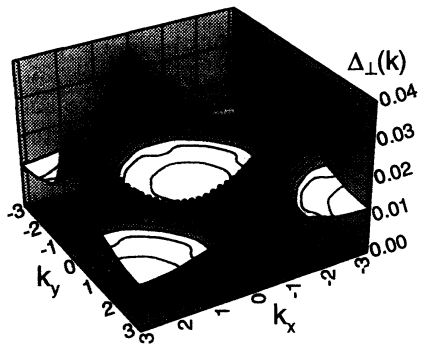

FIG. 4. A contour plot of the gap $\Delta_\perp(\mathbf{k})$ for $x = 0.085$ and $J_\perp^0 = 0.2 J_\parallel^0$. The diamondlike Fermi surface is indicated by the black dotted line. Notice that the gap $\Delta_\perp(\mathbf{k})$ has an extended s-wave symmetry, with peaks at the four corners $\mathbf{k} = (\pm\pi, 0)$ and $\mathbf{k} = (0, \pm\pi)$, and without nodes. At the corners of the Fermi surface the gap is approximately $\Delta_\perp(\mathbf{k}) \simeq 0.032 J_\parallel^{\rm eff} \simeq 4$ meV. Also notice that $\Delta_\perp(\mathbf{k})$ is significantly larger at the Fermi surface than in the middle of the Brioullin zone.

(denoted by squares) and negative on the sublattice with r_x odd (denoted by diamonds). This alternating sign was anticipated in the previous section in Eq. (32). Also notice that $|\Delta_\perp(\mathbf{r})|$ is relatively large on the diagonal $\mathbf{r} = (j, j)$, which means that in momentum space $\Delta_\perp(\mathbf{k})$ will be enhanced along the diamond defined by $k_x \pm k_y = \pm\pi$.

In Fig. 4 we show a two-dimensional plot of $\Delta_\perp(\mathbf{k})$ in momentum space. Observe that $\Delta_\perp(\mathbf{k})$ is indeed enhanced at the Fermi surface, and that $\Delta_\perp(\mathbf{k})$ is especially large at the four corners of the Fermi surface. This anisotropy of $\Delta_\perp(\mathbf{k})$ is easier to see in Fig. 5, which shows a plot of $\Delta_\perp(\mathbf{k})$ around the Fermi surface for three different values of doping. Note that $\Delta_\perp(\mathbf{k})$ has an (extended) s-wave symmetry without nodes, and that the anisotropy

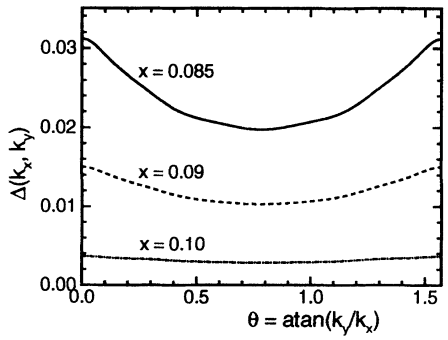

FIG. 5. The interplane gap $\Delta_\perp(\mathbf{k})$ around the Fermi surface for $x = 0.085$, $x = 0.09$ and $x = 0.10$. The gap $\Delta_\perp(\mathbf{k})$ has an extended s-wave symmetry, and is anisotropic around the Fermi surface, with peaks at the corners of the Fermi surface. This anisotropy is quite pronounced for $x = 0.085$, which is close to the AF instability at $x_c = 0.08$. At the corners of the Fermi surface the gap is approximately $0.032\ J_\parallel^{\rm eff} \simeq 4$ meV for $x = 0.085$. For higher doping $x = 0.09$ and $x = 0.10$ the amplitude of the gap decreases rapidly, and the anisotropy almost disappears. The conclusion is that the antiferromagnetic correlations are essential for the enhancement of $\Delta_\perp(\mathbf{k})$.

of $\Delta_\perp(\mathbf{k})$ is quite pronounced for $x = 0.085$, but less pronounced for $x = 0.09$ and $x = 0.10$. Let us first look at the results for $x = 0.085$ (solid line). At the corners of the Fermi surface the value of $\Delta_\perp(\mathbf{k})$ is approximately $0.032\ J_\parallel^0 \simeq 4$ meV. In the middle of the Fermi surface the gap is approximately two-third of this value. We also calculated the pairing transition temperature $T_P^\perp$ at $x = 0.085$, which gave the result $T_P^\perp \simeq 0.016 J_\parallel^0$, which is of the order of 20 K. We emphasize that these numbers depend strongly on the specific values of the parameters in the model, and how close the doping is to the critical value x_c. Although the magnitude of the gap $\Delta_\perp(\mathbf{k})$ is still too small, we believe it is plausible to identify the spin gap observed in $YBa_2Cu_3O_{6.6}$ with $\Delta_\perp(\mathbf{k})$, and the spin-gap phase transition with $T_P^\perp$. In Fig. 5 we also show $\Delta_\perp(\mathbf{k})$ for a slightly higher doping $x = 0.09$ and $x = 0.10$. Notice that further away from the critical doping $x_c = 0.08$ the magnitude of $\Delta_\perp(\mathbf{k})$ decreases rapidly, and the anisotropy of $\Delta_\perp(\mathbf{k})$ is less pronounced as well. This result shows that the antiferromagnetic correlations are essential to make interlayer pairing possible at a reasonably high-energy scale.

In the RPA treatment the antiferromagnetic correlations are tied to the band structure in a way that may not be quantitatively correct. To study the dependence of the gap $\Delta_\perp$ on the correlation length r_0 and the coupling constant $J_\perp^0$, we consider an effective interplane pairing parametrized by

$$J_\perp^{\rm eff}(\mathbf{r}) = J_\perp^0 (-1)^{i+j} e^{-r/r_0}, \tag{33}$$

where $\mathbf{r}/a = (i, j)$, and r_0 should be interpreted as the correlation length of the antiferromagnetic correlations. The dependence of the gap on the coupling constant $J_\perp^0$ is shown in Fig. 6, which is a logarithmic plot of $\Delta_\perp^{\rm max}$

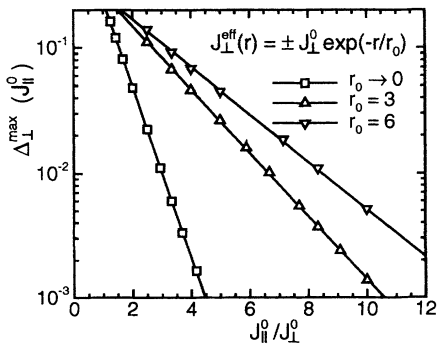

FIG. 6. A logarithmic plot of the gap $\Delta_\perp^{\rm max}$ at the corner of the Fermi surface as a function of the interplane coupling constant $(J_\perp^0)^{-1}$. In this calculation we assumed that the effective coupling is given by $J_\perp^{\rm eff}(\mathbf{r}) = \pm J_\perp^0 \exp(-r/r_0)$, and we fixed the doping at $x = 0.09$. We performed the calculations for a correlation length $r_0 = 3$ ($\triangle$) and $r_0 = 6$ ($\triangledown$), and compared the results with an "on-site" interaction, which corresponds with $r_0 \to 0$ ($\square$). The straight lines show that $\Delta_\perp^{\rm max}$ depends exponentially on $(J_\perp^0)^{-1}$. The functional form is given in Eq. (34). Notice that for $r_0 = 3$ the slope of the line is 2.7 times smaller than for $r_0 \to 0$, and that therefore $\Delta_\perp^{\rm max}(r_0 = 3) \gg \Delta_\perp^{\rm max}(r_0 \to 0)$. The finite correlation length has the effect of enhancing $J_\perp^0$ by a factor of 2.7.

versus $(J_\perp^0)^{-1}$. We defined $\Delta_\perp^{\max}$ as the value of $\Delta_\perp(\mathbf{k})$ at the corner of the Fermi surface. We did the calculations for a correlation length $r_0 \to 0$ ($\square$), $r_0 = 3$ ($\triangle$), and $r_0 = 6$ ($\triangledown$). The case $r_0 \to 0$ is the situation when $J_\perp^{\text{eff}}(\mathbf{r})$ and $\Delta_\perp(\mathbf{r})$ are only nonzero for $\mathbf{r} = 0$, which corresponds to a pure s-wave symmetry. Observe that the data points lie on straight lines with different slopes. We conclude that $\Delta_\perp^{\max}(\mathbf{k})$ has the functional form

$$\Delta_\perp^{\max} \simeq \begin{cases} 1.14\, J_\parallel^0 \exp\left(-1.56\, J_\parallel^0/J_\perp^0\right) & \text{for } r_0/a \to 0, \\ 0.48\, J_\parallel^0 \exp\left(-0.58\, J_\parallel^0/J_\perp^0\right) & \text{for } r_0/a = 3, \\ 0.41\, J_\parallel^0 \exp\left(-0.44\, J_\parallel^0/J_\perp^0\right) & \text{for } r_0/a = 6. \end{cases} \tag{34}$$

This BCS-like functional form is not surprising, because $\Delta_\perp(\mathbf{k})$ is determined in a way that is very similar to BCS theory. Notice however that the coefficients Eq. (34) change dramatically when the correlation length r_0/a increases from 0 to 3. For $r_0/a \gtrsim 3$ these coefficients do not change much anymore, because the system can only take advantage of very long correlation lengths if there is perfect nesting of the Fermi surface. This calculation was done at a finite doping $x = 0.09$, and thus the nesting is not perfect. First consider the coefficient in the exponent, which drops from 1.56 to 0.58 when r_0/a increases from 0 to 3. The physical explanation for this is that when patches of spins cooperate to form extended Cooper pairs, $J_\perp^0$ gets effectively renormalized by a factor which increases with r_0/a. This renormalized $J_\perp'$ is the coupling constant that enters the exponent in Eq. (34), i.e., $J_\perp' = \frac{1.56}{0.58} J_\perp^0 \sim 3J_\perp^0$ for $r_0/a = 3$. Now consider the prefactor in Eq. (34), which is proportional to $J_\parallel^0$. In BCS theory this prefactor would be equal to the Debye frequency, which provides a cutoff in the energy integrations. In the calculation that led to Eq. (34) there was no cutoff in the energy integrations, and so the Debye frequency is replaced by $J_\parallel^0$, the overall energy scale. If the correlation length r_0 increases, an effective energy cutoff is introduced, because $\Delta_\perp(\mathbf{k})$ becomes anisotropic with peaks that have a width proportional to a/r_0. Therefore the "Debye frequency" $J_\parallel^0$ gets replaced by roughly $(a/r_0)J_\parallel^0$. We would like to mention that this calculation did not take any frequency dependence of $J^{\text{eff}}(\mathbf{q},\omega)$ into account. Millis and Monien argued that the frequency dependence of $J^{\text{eff}}(\mathbf{q},\omega)$ introduces another cutoff in the energy integrations, of the order of $(a/r_0)^2 J_\parallel^0$,[4,22] and is therefore more important than the cutoff provided by the momentum dependence of $J^{\text{eff}}(\mathbf{q},\omega)$. This argument does not modify the coefficients in the exponents in Eq. (34), and thus $\Delta_\perp^{\text{eff}}$ is still strongly enhanced when the correlation length increases.

V. PAIR-BREAKING EFFECTS OF THE GAUGE FIELD

We have argued in a previous paper that for a single CuO_2 plane a fluctuating gauge field destroys the in-plane pairing order parameter $\Delta_\parallel$ above the Bose-condensation temperature T_{BE}.[12] This explains the absence of a spin-gap phase in single-layer materials. In this section we will argue that the gauge field is not as effective in destroying the interplane order parameter $\Delta_\perp$, so that the spin gap can survive in multilayer materials.

In the previous sections we discussed a mean-field approximation of the t-J model. To go beyond mean-field theory we will now introduce a gauge field that takes a certain class of fluctuations around the mean-field result into account. The gauge field is the phase of the RVB-order parameter

$$\xi_{ij} = \xi e^{ia_{ij}}, \tag{35}$$

where ξ is given by Eq. (7). We refer to other papers for a more comprehensive discussion of the properties of this gauge field a_{ij}.[7–10,12,23] In our model for two CuO_2 planes there are two gauge-field modes per unit cell, because each plane has its own gauge field, denoted by $a_{ij}^{(1)}$ and $a_{ij}^{(2)}$. Suppose that the two planes are coupled by a nonzero interplane order parameter $\Delta_\perp$, as described by the Hamiltonian in Eq. (21). In that case the two gauge-field modes are coupled as well, and the total gauge-field action has the form

$$S[a] = \frac{T}{2} \sum_q \left(\delta_{\alpha\beta} - \frac{q_\alpha q_\beta}{q^2}\right) \begin{pmatrix} a_q^{(1)\alpha} \\ a_q^{(2)\alpha} \end{pmatrix}^\dagger \times \begin{bmatrix} \Pi_\parallel(q) & \Pi_\perp(q) \\ \Pi_\perp(q) & \Pi_\parallel(q) \end{bmatrix} \begin{pmatrix} a_q^{(1)\beta} \\ a_q^{(2)\beta} \end{pmatrix}, \tag{36}$$

where q denotes $(\mathbf{q}, i\nu_n)$ and $i\nu_n$ is a Matsubara frequency. The propagators $\Pi_\parallel(q)$ and $\Pi_\perp(q)$ are given by the diagrams in Fig. 7. Notice that $\Pi_\perp(q) = 0$ when $\Delta_\perp = 0$, because in that case the two planes are uncoupled, and thus the diagram in Fig. 7(b) vanishes. The eigenmodes of the action in Eq. (36) are the *in-phase* mode $a_q^{(+)} \equiv (a_q^{(1)} + a_q^{(2)})/\sqrt{2}$ and the *out-of-phase* mode $a_q^{(-)} \equiv (a_q^{(1)} - a_q^{(2)})/\sqrt{2}$. We will denote the propagators of these two eigenmodes by $\Pi_\pm(q) \equiv \Pi_\parallel(q) \pm \Pi_\perp(q)$.

In order to decide whether the combined effect of the two gauge-field modes is pair breaking or not, one has to calculate the total free energy of each gauge-field mode, and study whether the free energy increases or not when a gap $\Delta_\perp$ opens up. This is outside the scope of this paper, and we will instead limit ourselves to qualitative

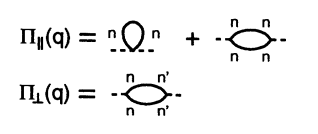

FIG. 7. The diagrams for the gauge field propagators $\Pi_\parallel(q)$ and $\Pi_\perp(q)$. The indices n and n' indicate plane 1 or plane 2 (and $n \neq n'$). The propagator $\Pi_\perp(q)$ is only nonzero if there is a coupling between the two planes. In Sec. V we show that the in-phase propagator $\Pi_+ = \Pi_\parallel + \Pi_\perp$ becomes massive when an interplane gap $\Delta_\perp$ opens up, while the out-of-phase propagator $\Pi_- = \Pi_\parallel - \Pi_\perp$ remains massless.

arguments why it is less costly to have an interplane gap $\Delta_\perp$ than to have an in-plane gap $\Delta_\parallel$. Our qualitative argument is based on the fact that in the case of interplane pairing one of the two gauge-field modes remains massless, while in the case of in-plane pairing both modes become massive. The fact that a certain mode becomes massive is generally an indication that this mode is pair breaking.

Evaluating the diagrams in Fig. 7 in the presence of an interplane gap $\Delta_\perp(\mathbf{k})$ gives

$$\Pi_\pm(\mathbf{q}, i\nu_n) = C + 2T\sum_{i\omega_n}\int \frac{d^2k}{(2\pi)^2}\left(\hat{\mathbf{q}}\times\frac{\partial\epsilon}{\partial\mathbf{k}}\right)\left(\hat{\mathbf{q}}\times\frac{\partial\epsilon'}{\partial\mathbf{k}}\right) \times\frac{\epsilon\epsilon' - \omega_n\omega_n' \pm \Delta\Delta'}{(\omega_n^2+E^2)(\omega_n'^2+E'^2)}, \tag{37}$$

where $i\omega_n' = i\omega_n - i\nu_n$, $\epsilon, \epsilon' = \epsilon_{k\pm q/2}$, $\Delta, \Delta' = \Delta_\perp(\mathbf{k}\pm\mathbf{q}/2)$, and $E = \sqrt{\epsilon^2+\Delta^2}$. The first term in Eq. (37) is a constant given by the first diagram in Fig. 7(a), which is equal to

$$C = 2T\sum_{i\omega_n}\int \frac{d^2k}{(2\pi)^2}\frac{\partial^2\epsilon_k}{\partial\mathbf{k}^2}\frac{\epsilon_k}{E_k^2+\omega_n^2}. \tag{38}$$

For $\Delta = 0$ this constant C exactly cancels the second term in Eq. (37) for $\mathbf{q}\to 0$ and $i\nu_n = 0$. Thus the gauge field is massless in the normal state. Note that the functional form of the in-phase propagator $\Pi_+(q)$ is similar to the BCS expression for the propagator of the electromagnetic gauge field in the presence of a gap,[24] except that the coupling constants are very different. It is very well known that this propagator becomes massive when a gap opens up, i.e., $\Pi_+(0,0)\propto\Delta_\perp^2$, which is responsible for the Meissner effect in BCS superconductors.

The out-of-phase mode $a_q^{(-)}$, on the other hand, has a propagator $\Pi_-(q)$ with a different coherence factor, proportional to $\epsilon\epsilon' - \omega_n\omega_n' - \Delta\Delta'$. One can easily check that due to the minus sign in the coherence factor the second term in Eq. (37) exactly cancels the constant C in Eq. (38) in the limit $\mathbf{q}\to 0$ and $i\nu_n = 0$, even when $\Delta\neq 0$. In other words, the out-of-phase propagator $\Pi_-(q)$ remains massless when an interlayer gap opens up. The physical reason why the out-of-phase mode $a_q^{(-)}$ remains massless is related to gauge invariance. Without pairing the Hamiltonian is invariant under the local gauge transformation

$$f_{j\sigma}^{(n)} \longrightarrow e^{i\varphi_j^{(n)}} f_{j\sigma}^{(n)}, \tag{39}$$

$$a_{ij}^{(n)} \longrightarrow a_{ij}^{(n)} - \varphi_i^{(n)} + \varphi_j^{(n)}. \tag{40}$$

A finite gap Δ generally breaks this gauge invariance, which implies that the gauge-field mode becomes massive. This is usually refered to as the Higgs mechanism. In order to see what happens to the out-of-phase gauge-field mode $a_q^{(-)}$, we only consider gauge transformations that satisfy $\varphi_i^{(1)} = -\varphi_i^{(2)}$. One immediately observes that the interplane order parameter $\Delta_\perp = \langle f_{i\uparrow}^{(1)} f_{i\downarrow}^{(2)} - f_{i\downarrow}^{(1)} f_{i\uparrow}^{(2)}\rangle$ is invariant under this class of gauge transformations. The Higgs mechanism does not apply because the gauge invariance is not broken, and therefore the out-of-phase gauge-field mode $a_q^{(-)}$ remains massless.

For a more detailed analysis of the pair-breaking effects of the gauge-field modes $a^{(+)}$ and $a^{(-)}$, one has to study the contribution of the gauge field to the free energy, given by[25,12]

$$F_{\text{gauge}}^{(\pm)} = T\sum_{\mathbf{q},\nu_n}\log\Pi_\pm(\mathbf{q}, i\nu_n) = \sum_{\mathbf{q}}\int_0^\infty\frac{d\nu}{2\pi}[2n_B(\nu)+1] \times\arctan\left(\frac{\operatorname{Im}\Pi_\pm(\mathbf{q},\nu+i\delta)}{\operatorname{Re}\Pi_\pm(\mathbf{q},\nu+i\delta)}\right). \tag{41}$$

In the normal state the gauge field gives a rather large negative contribution to the free energy. It has been shown that the free energy from free fermions and bosons is much too large, and that the negative contribution from the transverse and longitudinal gauge fluctuations yields a free energy which is in much better agreement with high-temperature expansions.[25]

Let us now ask what happens when a gap opens up in the fermion spectrum. We can calculate $F_{\text{gauge}}^{(\pm)}(\Delta)$ by substituting the propagator $\Pi_\pm(\mathbf{q},\nu,\Delta)$ into Eq. (41). Let us first consider $F_{\text{gauge}}^{(+)}(\Delta)$. For $\Delta\neq 0$ a gap appears in $\operatorname{Im}\Pi_\pm(\mathbf{q},\nu)$, eliminating the contribution of modes with $\nu < 2\Delta$. For $\nu > 2\Delta$, $-(\operatorname{Im}\Pi_+/\operatorname{Re}\Pi_+)$ is still suppressed compared to its normal state value, causing a significant increase in $F_{\text{gauge}}^{(+)}(\Delta)$. It was shown in Ref. 12 that $F_{\text{gauge}}^{(+)}(\Delta)\propto\Delta^{5/3}$ if $T > T_{\text{BE}}$. This cost in free energy is so large that it destroys the possibility of fermion pairing for $T > T_{\text{BE}}$, thereby eliminating the spin-gap phase in single-layer cuprates.

The story is quite different for $F_{\text{gauge}}^{(-)}(\Delta)$. Again a gap appears in $\operatorname{Im}\Pi_-(\mathbf{q},\nu)$, but for $\nu > 2\Delta$ the coherence factor in Eq. (37) is such that $-(\operatorname{Im}\Pi_-/\operatorname{Re}\Pi_-)$ is actually *enhanced*,[12] which overwhelms the loss of free energy from frequencies $\nu < 2\Delta$. Considering that $F_{\text{gauge}}^{(-)}(\Delta)$ decreases when a gap opens up, we conclude that the gauge-field mode $a_q^{(-)}$ is pair enhancing. The pair-enhancing nature of $a_q^{(-)}$ can also be understood in another way.[26] The fermions on the two planes couple to the $a^{(-)}$ mode with opposite charge, so that the exchange of an $a^{(-)}$ mode leads to an attraction, analogous to what happens in the t-t'-J model.[27] In our case we expect that the effects of the $a_q^{(+)}$ and $a_q^{(-)}$ gauge fluctuations largely cancel each other, so that the mean-field treatment of interplane pairing may be quite reliable. As a result it is likely that over a certain temperature range the in-plane gap $\Delta_\parallel(\mathbf{k})$ is completely destroyed by gauge-field fluctuations, while the interplane gap $\Delta_\perp(\mathbf{k})$ still survives. This region can be identified with the spin-gap phase.

VI. NMR-RELAXATION RATES

Experiments on $YBa_2Cu_3O_{6.6}$ show that quantities that probe the spin degrees of freedom of the system,

such as the NMR-relaxation rate T_1^{-1}, the echo-decay rate T_2^{-1}, and the Knight shift, are strongly reduced below a certain crossover temperature. In this section we will show that our model can reproduce the unusual temperature dependence of these quantities. The two main ingredients to obtain our results are the presence of strong antiferromagnetic correlations and the opening of a spin gap $\Delta_\perp$ due to the pairing of fermions on adjacent CuO_2 planes. We will mainly focus on the calculation of the NMR-relaxation rate $(T_1T)^{-1}$, whose temperature dependence contains information about both the magnitude of the spin gap and the presence of antiferromagnetic correlations.

The NMR-relaxation rate is directly related to the susceptibility according to the formula

$$\frac{1}{T_1T} = \frac{1}{\mu_B^2\hbar}\sum_{\mathbf{q}} F(\mathbf{q}) \lim_{\omega\to\infty} \frac{\chi''_{\rm phys}(\mathbf{q},\omega)}{\omega}. \tag{42}$$

The form factor $F(\mathbf{q})$ depends on the direction of the magnetic field, and whether one probes the copper sites or the oxygen sites. Following Millis *et al.*[28] and Monien *et al.*,[29] the form factors are given by

$$\begin{aligned} {}^{63}F_\parallel(\mathbf{q}) &= \frac{3}{8}\left[A_\parallel + 2B(\cos q_x a + \cos q_y a)\right]^2 \\ &\quad + \frac{3}{8}\left[A_\perp + 2B(\cos q_x a + \cos q_y a)\right]^2 , \\ {}^{63}F_\perp(\mathbf{q}) &= \frac{3}{4}\left[A_\perp + 2B(\cos q_x a + \cos q_y a)\right]^2 , \\ {}^{17}F(\mathbf{q}) &= \frac{3}{2}C^2(1+\cos q_x a), \end{aligned} \tag{43}$$

where "63" denotes the ^{63}Cu site, and "17" denotes the ^{17}O site. The constants $A_\parallel$, $A_\perp$, and C are approximately equal to[29]

$$\begin{aligned} A_\parallel &= -4B, \\ A_\perp &= 0.84B, \\ C &= 1.68B, \end{aligned} \tag{44}$$

and $B \simeq 40.8$ kOe/μ_B. The main feature of these form factors is that ${}^{17}F(\mathbf{q})$ vanishes at $\mathbf{q} = (\pi,\pi)$, while ${}^{63}F_\parallel(\mathbf{q})$ has its maximum at $\mathbf{q} = (\pi,\pi)$. This implies that the relaxation rate on the copper sites will be strongly enhanced due to antiferromagnetic correlations, while this enhancement will not be seen in $({}^{17}T_1T)^{-1}$.

In order to find $(T_1T)^{-1}$ we will use the RPA approximation to calculate the susceptibility $\chi_{\rm phys}(\mathbf{q},\omega)$. Within the RPA approximation one can express $\chi^{\rm RPA}_{\rm phys}$ in terms of the bare susceptibility $\chi^0(\mathbf{q},\omega)$, similar to the expression in Eq. (15). The only difference is that we now have a finite spin gap $\Delta_\perp(\mathbf{k})$ coupling the two planes, which implies that the bare susceptibility $\chi^0(\mathbf{q},\omega)$ is now a 2×2 matrix instead of a number. Following the derivation of Eq. (15), and replacing χ^0 by a 2×2 matrix $\boldsymbol{\chi}^0$ at each step, we obtain

$$\chi_{\rm phys}(\mathbf{q},q_z,\omega) = \left[\frac{\cos^2(\frac{1}{2}q_z d)}{1+J_+\chi_+} + \frac{\sin^2(\frac{1}{2}q_z d)}{1+J_-\chi_-}\right]\chi_+(\mathbf{q},\omega), \tag{45}$$

where

$$\begin{aligned} \chi_\pm &= \chi^0_\parallel \pm \chi^0_\perp, \\ J_\pm &= J_\parallel \pm J_\perp. \end{aligned} \tag{46}$$

[For $\chi_+ = \chi_- = \chi^0$ this reduces to the expression in Eq. (15).] The susceptibilities $\chi_\pm$ are determined by evaluating a single fermion bubble, which gives[24,30]

$$\begin{aligned} \chi_\pm(\mathbf{q},\omega+i\delta) = \int \frac{d^2k}{(2\pi)^2}\frac{1}{2}\Bigg[& l_\pm^2 \frac{f(E')-f(E)}{E-E'+\omega+i\Gamma} \\ & + p_\pm^2 \frac{1-f(E')-f(E)}{E+E'+\omega+i\Gamma}\Bigg] \\ & + [\omega+i\Gamma \to -(\omega+i\Gamma)], \end{aligned} \tag{47}$$

where $\epsilon = \epsilon_{k+q/2}$, $\epsilon' = \epsilon_{k-q/2}$, and $E = \sqrt{\epsilon^2+\Delta^2}$. The coherence factors $l_\pm^2$ and $p_\pm^2$ are defined by

$$\begin{aligned} l_\pm^2 &= \tfrac{1}{2}\left(1 + \tfrac{\epsilon\epsilon' \pm \Delta\Delta'}{EE'}\right), \\ p_\pm^2 &= \tfrac{1}{2}\left(1 - \tfrac{\epsilon\epsilon' \pm \Delta\Delta'}{EE'}\right). \end{aligned} \tag{48}$$

In BCS theory one only obtains the "plus" coherence factors l_+^2 and p_+^2.[24] In our case the "minus" coherence factors l_-^2 and p_-^2 are due to the fact that the pairing is between fermions on different planes, which can be in phase or out of phase with each other.

We included a finite scattering rate Γ in the expression for $\chi_\pm$,[30] in order to remove a logarithmic singularity in $\chi''_\pm(\mathbf{q},\omega)/\omega$ in the limit $\omega \to 0$. In conventional superconductors this logarithmic singularity, cut off by a small scattering rate $\Gamma \ll T$, is responsible for the Hebel-Slichter peak in $(T_1T)^{-1}$ just below the pairing transition temperature. For the cuprates it is well known that there is an anomalously large scattering rate Γ, which can be a sizable fraction of the temperature T. Within our treatment of the t-J model this scattering rate is due to strong gauge-field fluctuations.[10] The large value of Γ implies that the Hebel-Slichter peak will be significantly smaller in the cuprates than in conventional superconductors.

Before presenting our numerical results, we will first discuss the value of the gap $\Delta_\perp(\mathbf{k})$ that enters the calculation of $\chi_\pm(\mathbf{q},\omega)$. The gap $\Delta_\perp$ has to be quite large in order to identify $\Delta_\perp$ with the temperature scale below which $(T_1T)^{-1}$ decreases, which happens at about 150 K for underdoped $YBa_2Cu_3O_{6.6}$. As was discussed in Secs. III and IV, the interplane gap $\Delta_\perp(\mathbf{k})$ is strongly enhanced by the antiferromagnetic correlations in underdoped cuprates. Within our RPA treatment we can only obtain a sufficiently large value for $\Delta(\mathbf{k})$ if the doping is very close to the critical doping $x_c \simeq 0.08$ at which the antiferromagnetic instability occurs. However, experiments show that the antiferromagnetic correlations remain rather strong over a wide range of doping. Unfortunately the RPA approximation is not powerful enough to capture this physics. We will therefore in this section use a value of $\Delta_\perp$ that fits the observed temperature dependence of $(T_1T)^{-1}$, keeping in mind that the antiferromagnetic correlations are responible for such a large value of the gap. Although $\Delta_\perp(\mathbf{k})$ is anisotropic around the Fermi surface, this anisotropy does not play an important role in the calculations below. The rea-

son for this is that the expression for $(T_1T)^{-1}$ is dominated by wave vectors $\mathbf{q} \simeq \mathbf{Q}_{\rm AF}$, and the integrand for $\chi_{\pm}(\mathbf{Q}_{\rm AF}, 0)$ is only large when $\mathbf{k} + \frac{1}{2}\mathbf{Q}_{\rm AF}$ and $\mathbf{k} - \frac{1}{2}\mathbf{Q}_{\rm AF}$ are both on the Fermi surface. This condition is only satisfied when $\mathbf{k} \pm \frac{1}{2}\mathbf{Q}_{\rm AF} = \pm\frac{1}{2}\mathbf{Q}_{\rm AF}$. Thus we can safely put $\Delta_\perp = \Delta_\perp(\frac{1}{2}\mathbf{Q}_{\rm AF})$ in the calculation of $(T_1T)^{-1}$. Notice that it is important that $\Delta_\perp(\mathbf{k})$ has an (extended) s-wave symmetry, because $\Delta_\perp(\frac{1}{2}\mathbf{Q}_{\rm AF})$ would nearly vanish if $\Delta_\perp(\mathbf{k})$ had a d-wave symmetry.

We will now discuss the temperature dependence of the gap $\Delta_\perp(T)$. The most straightforward approximation would be to assume that $\Delta_\perp$ is a mean-field order parameter with a BCS-like temperature dependence. In that case $\Delta_\perp(T) = 0$ for $T > T_P$, and $\Delta_\perp(T)$ increases with an infinite slope just below T_P, as is shown in the insert in Fig. 8. However, this BCS picture assumes that there is a long coherence length, so that $\Delta_\perp$ can be interpreted as a long-range order parameter. As was pointed out by McMillan,[31] this is not the appropriate picture if there is a relatively short coherence length, which is clearly the case for cuprates in the spin-gap phase. If the coherence length is small the long-range order parameter $\langle\Delta_\perp(\mathbf{r})\rangle$ vanishes, and instead one should identify the gap with the *local* order parameter $\langle|\Delta_\perp(\mathbf{r})|^2\rangle$. Thus we are not dealing with a true gap, but with a *pseudogap*. This implies that there is not a sharp transition at which the gap disappears, because above the mean-field transition temperature the local order parameter $\langle|\Delta_\perp(\mathbf{r})|^2\rangle$ remains nonzero. This is indicated by the insert in Fig. 9, which shows a tail in the pseudogap $\Delta_\perp$ for $T > T_P^0$. For most purposes this tail in $\Delta_\perp(T)$ is not very important, because it will be washed out by thermal fluctuations. However, the tail in $\Delta_\perp(T)$ will have a significant effect on the Hebel-Slichter peak in $(T_1T)^{-1}$, which will be smeared out if the gap $\Delta_\perp(T)$ is smoothly varying instead of dropping down to zero at $T = T_P$. This can explain the absence of a Hebel-Slichter peak for the high-T_c cuprates at the onset of the spin-gap phase.

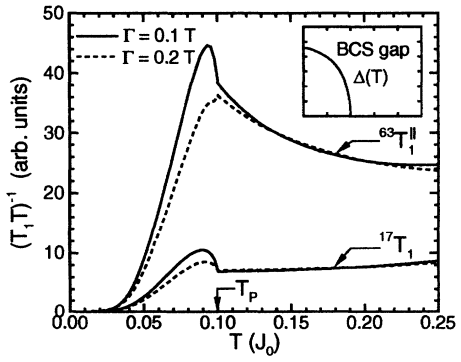

FIG. 8. The NMR-relaxation rate $(T_1T)^{-1}$ on the copper and the oxygen sites for two values of the scattering rate Γ. This calculation uses a BCS-like temperature dependence for the spin gap $\Delta_\perp(T)$. The Hebel-Slichter peak gets less pronounced when Γ increases. For $T > T_P$ the relaxation rate $(^{63}T_1^{\parallel}T)^{-1}$ rises when T decreases, while $(^{17}T_1T)^{-1}$ remains constant. This rise in $(^{63}T_1^{\parallel}T)^{-1}$ is due to antiferromagnetic correlations. Notice that there is a sharp change in behavior for $T < T_P$ and $T > T_P$, which is not observed in experiments.

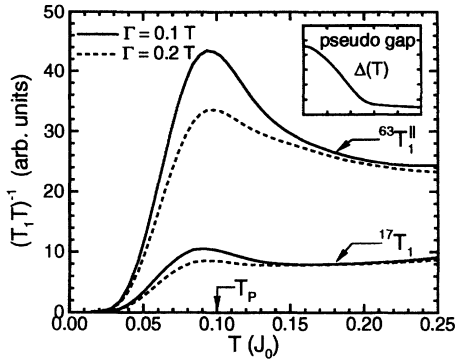

FIG. 9. The NMR-relaxation rate $(T_1T)^{-1}$ on the copper and the oxygen sites, using a pseudogap $\Delta_\perp(T)$ which has a finite tail for $T > T_P^0$, as is shown in the inset. The main difference with Fig. 8 is that the Hebel-Slichter peak gets smeared out over a wider range of temperature. As a result $(T_1T)^{-1}$ varies smoothly as a function of temperature, which agrees well with measurements on underdoped $YBa_2Cu_3O_{6.6}$.

In Fig. 8 we show plots of the NMR-relaxation rate $(T_1T)^{-1}$ on the copper and the oxygen sites for various values of the scattering rate Γ. This calculation assumes a BCS-like behavior for the gap $\Delta_\perp(T)$, and T_P is chosen to be equal to $0.1J$. For small values of the scattering rate Γ the Hebel-Slichter peak is quite pronounced, but the size of this peak gets smaller and smaller when Γ increases. However, even for a large value of Γ one still observes a drastic change in the behavior of $(T_1T)^{-1}$ when T crosses the transition temperature T_P. Also notice that for $T > T_P$, $(^{63}T_1T)^{-1}$ increases when T decreases, while $(^{17}T_1T)^{-1}$ remains almost constant. The reason for this difference is that the form factor $^{63}F(\mathbf{q})$ is finite at $\mathbf{q} = (\pi, \pi)$, while $^{17}F(\mathbf{q})$ vanishes at $\mathbf{q} = (\pi, \pi)$ according to Eq. (43). Therefore only the copper sites can take full advantage of the enhancement of $\chi''_{\rm phys}(\mathbf{q}, \omega)$ for $\mathbf{q} \simeq \mathbf{Q}_{\rm AF}$, which becomes stronger and stronger at lower temperatures.

In Fig. 9 we again show $(T_1T)^{-1}$ as a function of temperature, but this time we assumed that $\Delta_\perp(T)$ has a finite tail for $T \gtrsim T_P^0$, as is shown in the inset. The main difference between Figs. 8 and 9 is that the tail in $\Delta_\perp(T)$ smears out the Hebel-Slichter peak. As a result the temperature dependence of $(T_1T)^{-1}$ in Fig. 9 is smooth over the entire temperature range, which agrees much better with experiments than the plots in Fig. 8. As explained earlier in this section, we think that a tail in the pseudogap $\Delta_\perp(T)$ is closer to the truth than a BCS-like behavior of $\Delta_\perp(T)$.

We now turn to the calculation of the spin echo-decay rate T_2^{-1}, which has been measured experimentally by Takigawa.[32] It is given theoretically by[33]

$$\frac{1}{T_2} \propto \left(\sum_{\mathbf{q}} \chi_{\rm phys}(\mathbf{q}, 0)^2\right)^{1/2}. \tag{49}$$

In Fig. 10 we plot T_2^{-1} versus temperature for various values of the scattering rate Γ. Notice that in contrast to Figs. 8 and 9, introducing a finite Γ does not mod-

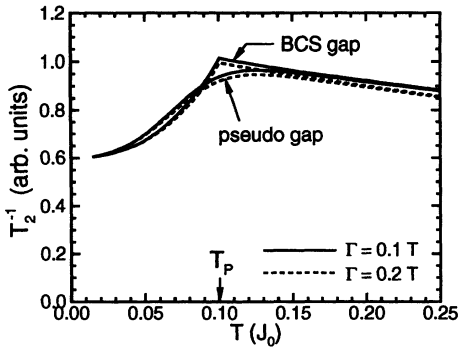

FIG. 10. The echo-decay rate T_2^{-1} as a function of temperature for two values of the scattering rate Γ. The dashed lines assume a BCS-like temperature dependence of the spin gap $\Delta_\perp(T)$, and the solid lines assume a pseudogap behavior. The tail in the pseudogap removes the singular behavior of T_2^{-1} at $T = T_P$. Changing the value of Γ does not have a significant effect on the behavior of T_2^{-1}.

ify T_2^{-1} significantly. Comparing the solid lines and the dashed lines we see that a tail in the pseudogap $\Delta_\perp(T)$ smears out the singular behavior of T_2^{-1} at $T = T_P^0$. Notice that for $T > T_P^0$, the echo-decay rate T_2^{-1} increases upon lowering T, which is due to antiferromagnetic correlations. This resembles the temperature dependence of $(^{63}T_1T)^{-1}$ in Fig. 9. However, for $T < T_P^0$ the temperature dependences of $(T_1T)^{-1}$ and T_2^{-1} are very different, because $(T_1T)^{-1}$ vanishes exponentially for $T \to 0$, while T_2^{-1} remains finite.

For completeness we show in Fig. 11 the temperature dependence of the Knight shift, which is proportional to $\chi_{\rm phys}(\mathbf{q} \to 0, \omega = 0)$. This quantity essentially probes the density of states around the Fermi surface, and vanishes exponentially when a spin gap opens up. We conclude that our calculation of T_1^{-1}, T_2^{-1} and $\chi_{\rm phys}(0,0)$ exhibits spin-gap behavior qualitatively similar to experiments, and that in order to explain the onset of the spin gap at 150 K$\simeq$ 0.1 $J_\parallel^0$, a spin gap of the order $\Delta_\perp \simeq 0.2\, J_\parallel^0$ is required.

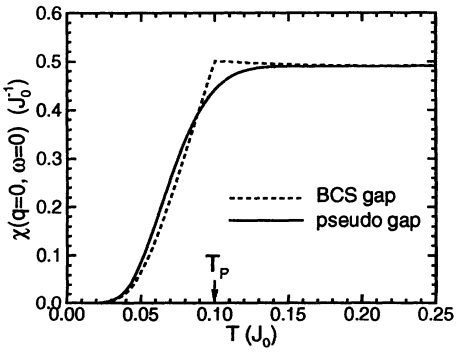

FIG. 11. The Knight shift as a function of temperature. In this calculation we used $\Gamma = 0$. The dashed line assumes a BCS-like temperature dependence of the spin gap $\Delta_\perp(T)$, and the solid line assumes a pseudogap behavior. The Knight shift decays exponentially when $T \lesssim \Delta_\perp(T)$.

VII. DISCUSSION

In this paper we studied a model for two CuO_2 planes, coupled with a small antiferromagnetic interplane interaction $J_\perp^0 \sum_i \mathbf{S}_i^{(1)} \cdot \mathbf{S}_i^{(2)}$. This model is relevant for multilayered high-T_c cuprates that have two (or more) CuO_2 planes in a unit cell.

Using a random-phase approximation we showed that close to half filling the susceptibility $\chi_{nn'}^{\rm RPA}(\mathbf{q}, q_z)$ is strongly peaked at the the nesting vector $\mathbf{q} \simeq \mathbf{Q}_{\rm AF}$, due to short-range antiferromagnetic correlations of the spins in each plane. Our expression for $\chi^{\rm RPA}(\mathbf{q}, q_z)$ explains the strong modulations as a function of q_z that have been observed in neutron scattering experiments for underdoped cuprates.[1] Within the same RPA analysis we showed that the effective coupling constants $J_\parallel^{\rm eff}(\mathbf{r})$ and $J_\perp^{\rm eff}(\mathbf{r})$ are also strongly enhanced by antiferromagnetic correlations. As a result $J_\parallel^{\rm eff}(\mathbf{r})$ and $J_\perp^{\rm eff}(\mathbf{r})$ can extend over several lattice spacings. Close to the AF instability $J_\parallel^{\rm eff}$ and $J_\perp^{\rm eff}$ become comparable in strength, because $J_\perp^{\rm eff}(\mathbf{q})$ is stronger enhanced than $J_\parallel^{\rm eff}(\mathbf{q})$ for $\mathbf{q} \simeq \mathbf{Q}_{\rm AF}$.

Due to the fact that the interplane coupling $J_\perp^{\rm eff}(\mathbf{r})$ is longer ranged, the system can form Cooper pairs that consist of fermions that are separated by several lattice spacings, characterized by the order parameter $\Delta_\perp(\mathbf{r})$. We solved the self-consistency equations for the order parameters $\Delta_\perp(\mathbf{r})$, and found that the interplane pairing is indeed strongly enhanced by the antiferromagnetic correlations. An interesting aspect is that the gap $\Delta_\perp(\mathbf{k})$ has an extended s-wave symmetry without nodes. A similar treatment of the in-plane pairing would lead to a gap $\Delta_\parallel(\mathbf{k})$ with an extended d-wave symmetry with nodes at four points on the Fermi surface. The gap $\Delta_\perp(\mathbf{k})$ is enhanced close to the Fermi surface, and is in particular large at the corners of the Fermi surface. How much can we trust the numbers that come out of this calculation? First of all the value of the gap is quite sensitive on the exact value of the parameters of the model. One also has to keep in mind that the RPA approximation is a gross oversimplification when the system is close to an AF instability. We can however state that our results are in qualitative agreement with the observed spin gap in underdoped $YBa_2Cu_3O_{6.6}$.

We propose that the enhanced interplane pairing provides a mechanism for the observed spin-gap phase in multilayer cuprates. To support this we argued that the gauge field, which destroys the in-plane gap $\Delta_\parallel$ in a single CuO_2 plane close to half filling, is less effective in destroying the interplane gap $\Delta_\perp$. The physical argument for this is that the out-of-phase mode $a_q^{(-)} = (a_q^{(1)} - a_q^{(2)})/\sqrt{2}$ remains massless when the interplane gap $\Delta_\perp(\mathbf{k})$ opens up. This implies that the gauge-field mode $a_q^{(-)}$ is not pair breaking. A more detailed calculation in Ref. 12 of the free energy of a gauge field indicates that the gauge-field mode $a_q^{(-)}$ actually *favors* pairing, and will partly cancel the pair-breaking effects of the in-phase gauge field mode $a_q^{(+)} = (a_q^{(1)} + a_q^{(2)})/\sqrt{2}$. The physical consequence of this is that at low doping the interplane gap $\Delta_\perp(\mathbf{k})$ can survive at a higher temperature than the in-plane gap

$\Delta_{\|}(\mathbf{k})$. This makes it possible that interplane pairing is responsible for the observed spin-gap phase in multilayer cuprates.

Our model is able to explain the unusual temperature dependence of several physical quantities that are related to the spin susceptibility. We calculated the NMR-relaxation rate $(T_1T)^{-1}$, using a value of the interplane gap $\Delta_\perp$ that corresponds with the observed spin gap in underdoped $YBa_2Cu_3O_{6.6}$. Our numerical results show that at high temperatures $(^{63}T_1T)^{-1}$ increases when T decreases, while $(^{17}T_1T)^{-1}$ remains almost constant. Below the pairing transition temperature T_P, $(^{63}T_1T)^{-1}$ and $(^{17}T_1T)^{-1}$ both decrease rapidly. The Hebel-Slichter peak is reduced by the assumption of a pseudogap behavior and the presence of inelastic scattering, presumably due to gauge field fluctuations. The physical reason why there is a pseudogap instead of the usual BCS gap is because there is a rather short coherence length, so that the gap should be interpreted as a *local* order parameter,[31] which does not undergo any sharp transitions.

So far we have ignored any interlayer hopping of the form $t_\perp c_{i\sigma}^{(1)\dagger} c_{i\sigma}^{(2)}$. From the analog of Eq. (3) it is clear that ignoring $t_\perp$ is reasonable provided that $xt_\perp < J_\perp$. If this is violated, we expect interlayer pairing to be suppressed, but we have not studied this quantitatively. Not enough is known about $t_\perp$ and $J_\perp$, but our guess is that $xt_\perp$ and $J_\perp$ are comparable. However, even a small $t_\perp$ will lead to coherence between bosons on the two planes immediately below T_{BE}, so that the fermion pairing becomes genuine superconducting pairing between electrons on the two layers.

The possibility of interplane pairing has interesting consequences for the symmetry of the superconducting gap in bilayer materials. In Fig. 12 we show a schematic phase diagram for these materials, in which the thick solid line denotes the onset of superconductivity. At low temperatures the in-plane d-wave and the interplane s-wave pairing will coexist, giving rise to a quasiparticle dispersion $E(\mathbf{k}) = (\epsilon(\mathbf{k})^2 + \Delta_\pm(\mathbf{k})^2)^{1/2}$, where $\Delta_\pm(\mathbf{k}) = \Delta_\perp(\mathbf{k}) \pm \Delta_{\|}(\mathbf{k})$. If $\Delta_\perp$ is indeed as large as 150 K, as the experiments seem to indicate, it is likely

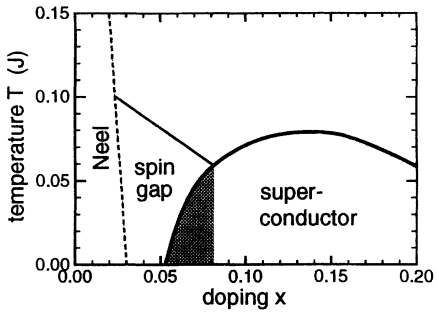

FIG. 12. A schematic phase diagram for bilayer cuprates. We predict that the spin-gap phase is due to interlayer fermion pairing, enhanced by antiferromagnetic correlations. Below the superconducting transition (thick solid line) the s-wave interplane pairing and the d-wave in-plane pairing coexist. We expect that for underdoped samples $\Delta_\perp(\mathbf{k})$ dominates over $\Delta_{\|}(\mathbf{k})$, giving rise to a nodeless superconducting state, indicated by the shaded region. At higher doping the four nodes of a d-wave superconductor are split into eight nodes.

that for underdoped materials $\Delta_\perp > |\Delta_{\|}|$ for all $\mathbf{k}$, which implies that the superconducting gap is nodeless. This is indicated by the shaded region in Fig. 12. As doping is increased, $\Delta_\perp$ decreases rapidly with the loss of antiferromagnetic correlations, and we cross over to a superconducting state with nodes. We expect that in fully doped systems the d-wave order parameter $\Delta_{\|}$ dominates, but as long as $\Delta_\perp$ remains finite the four nodes for a conventional d-wave superconductor will be split into eight nodes.

ACKNOWLEDGMENTS

We would like to thank Andy Millis for helpful discussions. This work was supported by the NSF through the Material Research Laboratory under Grant No. DMR-90-22933.

[1] J.M. Tranquada *et al.*, Phys. Rev. B **46**, 5561 (1992).
[2] B.J. Sternlieb *et al.*, Phys. Rev. B **47**, 5320 (1993).
[3] S. Shamoto *et al.*, Phys. Rev. B **48**, 13 817 (1993).
[4] A.J. Millis and H. Monien, Phys. Rev. Lett. **70**, 2810 (1993); **71**, 210(E) (1993).
[5] B.L. Altshuler and L.B. Ioffe, Solid State Commun. **82**, 253 (1992).
[6] P.W. Anderson, Science **235**, 1196 (1987); G. Baskaran, Z. Zou, and P.W. Anderson, Solid State Commun. **63**, 973 (1987).
[7] G. Baskaran and P.W. Anderson, Phys. Rev. B **37**, 580 (1988); G. Baskaran, Phys. Scr. T 27, 53 (1989).
[8] N. Nagaosa and P.A. Lee, Phys. Rev. Lett. **64**, 2450 (1990).
[9] N. Nagaosa and P.A. Lee, Phys. Rev. B **45**, 966 (1992).
[10] P.A. Lee and N. Nagaosa, Phys. Rev. B **46**, 5621 (1992).
[11] N. Nagaosa and P.A. Lee, Phys. Rev. B **43**, 1233 (1991).
[12] M.U. Ubbens and P.A. Lee, Phys. Rev. B **49**, 6853 (1994).
[13] L.B. Ioffe and G. Kotliar, Phys. Rev. B **42**, 10348 (1990).
[14] S. Sachdev, Phys. Rev. B **45**, 389 (1992).
[15] H. Fukuyama, Prog. Theor. Phys. Suppl. **108**, 287 (1992).
[16] J.M. Tranquada *et al.*, Phys. Rev. B **40**, 4503 (1989).
[17] A.E. Ruckenstein, P.J. Hirschfeld, and J. Appel, Phys. Rev. B **36**, 857 (1987).
[18] G. Kotliar and J. Liu, Phys. Rev. B **38**, 5142 (1988).
[19] I. Affleck and J.B. Marston, Phys. Rev. B **37**, 3774 (1988); J.B. Marston and I. Affleck, *ibid.* **39**, 11 538 (1989).
[20] M.U. Ubbens and P.A. Lee, Phys. Rev. B **46**, 8434 (1992).
[21] T. Tanamoto, H. Kohno, and H. Fukuyama, J. Phys. Soc. Jpn. **61**, 1886 (1992); **62**, 717 (1993).
[22] A.J. Millis, Phys. Rev. B **45**, 13 047 (1992).

[23] L.B. Ioffe and A.I. Larkin, Phys. Rev. B **39**, 8988 (1989).
[24] J.R. Schrieffer, *Theory of Superconductivity* (Addison-Wesley, Menlo Park, CA, 1964), Sec. 8-4.
[25] R. Hlubina, W.O. Putikka, T.M. Rice, and D.V. Khveshchenko, Phys. Rev. B **46**, 11 224 (1992).
[26] We are grateful to N. Bonesteel for a discussion on this point.
[27] P.B. Wiegmann, Phys. Rev. Lett. **60**, 821 (1988); Physica (Amsterdam) C **153-155**, 103 (1988); X.G. Wen, Phys. Rev. B **39**, 7223 (1989); P.A. Lee, Phys. Rev. Lett. **63**, 680 (1989).
[28] A.J. Millis, H. Monien, and D. Pines, Phys. Rev. B **42**, 167 (1990).
[29] H. Monien, D. Pines, and M. Takigawa, Phys. Rev. B **43**, 258 (1991).
[30] J.P. Lu, Phys. Rev. Lett. **68**, 125 (1992).
[31] W.L. McMillan, Phys. Rev. B **16**, 643 (1977).
[32] M. Takigawa, Phys. Rev. B **49**, 4158 (1994).
[33] A. Sokol and D. Pines, Phys. Rev. Lett. **71**, 2813 (1993).

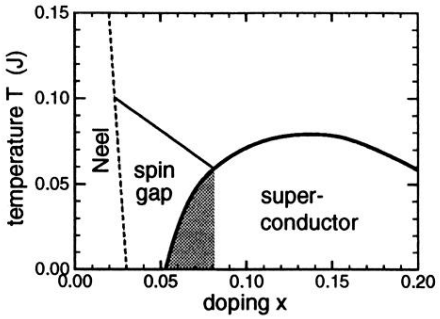

FIG. 12. A schematic phase diagram for bilayer cuprates. We predict that the spin-gap phase is due to interlayer fermion pairing, enhanced by antiferromagnetic correlations. Below the superconducting transition (thick solid line) the s-wave interplane pairing and the d-wave in-plane pairing coexist. We expect that for underdoped samples $\Delta_\perp(\mathbf{k})$ dominates over $\Delta_\parallel(\mathbf{k})$, giving rise to a nodeless superconducting state, indicated by the shaded region. At higher doping the four nodes of a d-wave superconductor are split into eight nodes.

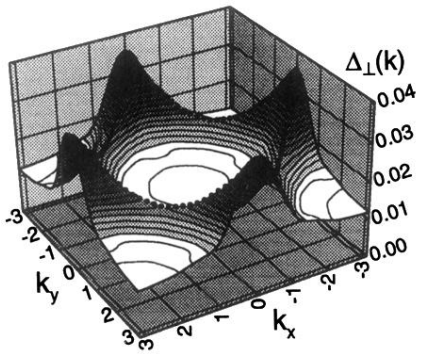

FIG. 4. A contour plot of the gap $\Delta_\perp(\mathbf{k})$ for $x = 0.085$ and $J_\perp^0 = 0.2J_\parallel^0$. The diamondlike Fermi surface is indicated by the black dotted line. Notice that the gap $\Delta_\perp(\mathbf{k})$ has an extended s-wave symmetry, with peaks at the four corners $\mathbf{k} = (\pm\pi, 0)$ and $\mathbf{k} = (0, \pm\pi)$, and without nodes. At the corners of the Fermi surface the gap is approximately $\Delta_\perp(\mathbf{k}) \simeq 0.032 J_\parallel^{\mathrm{eff}} \simeq 4$ meV. Also notice that $\Delta_\perp(\mathbf{k})$ is significantly larger at the Fermi surface than in the middle of the Brioullin zone.